Journal of Engineering and Technological Sciences

2-Dimensional Materials for Performance Enhancement of Surface Plasmon Resonance Biosensor: Review Paper

Chandra Wulandari^{1,2}, Ni Luh Wulan Septiani^{2,3,4}, Nugraha^{2,5}, Ahmad Nuruddin^{2,*} & Brian Yuliarto^{2,4,5}

¹Faculty of Industrial Technology, Institut Teknologi Bandung, Jalan Ganesa No. 10, Bandung 40132, Indonesia ²Advanced Functional Material Research Group, Faculty of Industrial Technology, Institut Teknologi Bandung, Jalan Ganesa No. 10, Bandung 41032, Indonesia

³Research Center for Advanced Materials, National Research and Innovation Agency (BRIN), Kawasan Puspiptek, South Tangerang 15134, Indonesia

⁴BRIN and ITB Collaboration Research Center for Biosensor and Biodevices, Institut Teknologi Bandung, Jalan Ganesa No. 10, Bandung 40132, Indonesia.

⁵Research Center for Nanosciences and Nanotechnology (RCNN), Institut Teknologi Bandung, Jalan Ganesa No. 10, Bandung 40132, Indonesia

Corresponding author: nuruddin@itb.ac.id

Abstract

Surface plasmon resonance (SPR)--based biosensors compete and excel among optical biosensors because of exceptional features such as high sensitivity, label-free, and real-time measurement, allowing the observation of molecular binding kinetics. In SPR biosensors and other biosensor techniques, surface functionalization and bioreceptor attachment are effective strategies to improve sensor performance. The application of an appropriate immobilization matrix for the bioreceptor is an essential step in maximizing the absorption of the bioreceptor on the sensor surface, thereby improving a specific target-sensor interaction. Furthermore, the materials should provide excellent optical properties to enhance the response signal. The high surface-to-volume ratio and high optical absorption of 2D materials qualify these requirements, thus promising advancements for SPR biosensors. This article reviews the recent SPR biosensor study with the use of the 2D materials family to improve the sensor performance, including graphene, transition metal dichalcogenides (TMDCs), MXene, black phosphorus (BP), perovskite, and boron nitride (BN). The materials properties and enhancement mechanisms of different 2D materials are discussed comprehensively. This review was expected to provide a future perspective and design approach for 2D materials-based SPR biosensors.

 $\textbf{Keywords:} \ 2D \ materials; immobilization \ matrix; optical \ biosensor; sensitivity \ enhancement; surface \ plasmon \ resonance.$

Introduction

Optical biosensors based on surface plasmon resonance (SPR) have been the interest of chemic sensor development in the last three decades due to their imperative features such as high sensitivity, real-time monitoring, quantitative measurement, minimal sample needs, label-free, and good reproducibility [1]. Since 1982, the first invention of SPR as a gas sensor [2], the application of SPR sensors has grown to various analytical needs in fields of environmental monitoring [3, 4], food safety [5, 6], medical diagnosis [7, 8], and laboratory medicine [9]. The simple configuration of SPR can be integrated into miniaturization. Thus, it is suitable for labon-a-chip (LOC) and point-of-care testing (POCT) applications [9, 10].

SPR relates to the phenomenon where collective electrons oscillate along the metal-dielectric interface, which excites the electromagnetic wave known as surface plasmon wave (SPW) [11]. In the dielectric and metal medium, the SPW propagating along the interface are transverse and exponentially decay. When the incident light excites the surface plasmon at the same propagation constant with SPW, it produces a resonance phenomenon called SPR [12, 13]. As the wave propagation depends on the dielectric constant, a slight change in the refractive index on the surface will change the SPR property, it can be represented by the angle or

Copyright © 2023 Published by IRCS - ITB ISSN: 2337-5779

J. Eng. Technol. Sci. Vol. 55, No. 3, 2023, 479-512 DOI: 10.5614/j.eng.technol.sci.2023.55.4.10

wavelength of resonances [14]. The sensitivity of the SPR to the changes in the refractive index is utilized for sensor applications. The basic principle of SPR is illustrated in Figure 1(a).

Figure 1(a) shows that a typical SPR biosensor chip consists of a metal thin film, commonly a gold-coated glass slide, modified with various materials and biomolecules, which are functionalized as immobilization matrices and bioreceptors, respectively. Bioreceptors provide the selectivity feature on the biosensors because the bioreceptors will interact with specific substances in the analyte [9]. The bioreceptors can be classified as antigen-antibodies [15], nucleic acid [16, 17], aptamers [18], enzymes [19], and artificial DNA [20]. The immobilization of those bioreceptors on the sensor surface is commonly realized by using the different interactions or reactions via some chemical linkers such as N,N'-bis-(6-maleimidylhexanoyl)cystamine (BMHC), (3-aminopropyl)triethoxysilane (APTES), etc. [21, 22]. However, the mentioned strategy is time-consuming and does not necessarily result in uniform immobilization [23].

The immobilization matrix on the SPR sensor was considered an alternative bioreceptor attachment method. A suitable immobilization matrix should possess a vast number of immobilization sites, strong adhesion, and retain the bio-functionality of bioreceptors [1, 24]. The availability of immobilization sites in a matrix is related to various surface properties such as surface area [25, 26], porosity [27], uniformity [22], and the availability of functional groups such as amino, thiol, hydroxyl, carboxyl, and aldehyde [26, 28, 29]. Furthermore, the electronic and optical properties of the matrix become important for improving SPR performances. Materials with high electron mobility, high optical absorption efficiency, and quantum confinement are fascinating and tremendous to be applied as a matrix in SPR sensors. The 2-dimensional (2D) materials have demonstrated remarkable electronic and optical properties owing to their thickness [30-34]. Flexible properties owned by the 2D structure allow the integration to various devices and systems easily [35, 36]. The properties can also be tuned by providing different treatments such as doping, decorating, mechanical modification, and external fields [30, 31]. Therefore, the utilization of 2D materials have attracted interest in various field of science and technology, especially in the development of SPR biosensors [25, 26, 37, 38].

Numerous studies have reported the utilization of 2D materials in SPR biosensors along with their advantages in improving sensing performance. However, to our knowledge, an integrated discussion covering various types of 2D materials in SPR biosensors still cannot be found elsewhere. In this article, we comprehensively discuss a recent study on SPR sensors using 2D materials, including graphene, transition metal dichalcogenides (TMDCs), and transition metal carbides/nitrides/carbonitrides (MXene), also how they have influenced the development of SPR sensors in the last decade. The significance of 2D materials for the sensitivity enhancement of the SPR biosensor is discussed. Further, various implementation and optimization strategies for 2D materials are described. This review also enlightens the mechanism between the 2D material and the SPR system, thereby improving the detection performance. Initially, the basic principle and developed technique used in SPR-based sensors is reviewed. Followed by the description of 2D materials characteristics and properties and their advantages for SPR biosensor application. The essence of the review is to discuss the reports related to 2D material-based SPR biosensors, which are divided into four categories as follows: (a) graphene, (b) TMDCs, (c) MXene, (d) others (including black phosphorus (BP), perovskite, and hexagonal boron nitride (h-BN)). This review may encourage the scientists and research community to pursue further study regarding 2D materials application for clinical application.

Principle and Technique of SPR-based Sensor

Surface plasmon resonance (SPR) is the resonance between surface plasmons (SPs) waves and incident light waves. The mechanism of SPR can be explained by Equations (1) and (2) below [39]. This condition is achieved when the propagation constant of SPs (k_{sp}) iequals the propagation constant of the incident light (k_x) . Surface plasmons (SPs) are collective oscillations of electrons at the interface of thin-film metals such as gold (Au) and silver (Ag) with the dielectric due to the difference in refractive index at the interface. Equation (1) shows the relationship between propagation constant SPs (k_{sp}) and propagation constant incident light in a vacuum medium (k_0) , with ε_m and ε_d as the dielectric constant of metal and dielectric, respectively. Based on Equation (1), the k_{sp} is always higher than the propagation constant of directly injected incident light to the metal and dielectric interface [40, 41]. Various techniques have been developed to enhance k_x , including optical

waveguide [42, 43], diffraction grating [44, 45], prism coupler [39, 46], and optical fiber. Through these approaches the k_x can be written as Equation (2). AFigure 1(b) shows that k_x is amplified and intersects with k_{sn} at a certain point, indicating surface plasmon excitation or SPR.

$$k_{sp} = k_0 \sqrt{\frac{\varepsilon_m \varepsilon_d}{\varepsilon_m + \varepsilon_d}} = \frac{2\pi}{\lambda} \sqrt{\frac{\varepsilon_m \times \varepsilon_d}{\varepsilon_m + \varepsilon_d}}$$
 (1)

$$k_x = k_0 \sqrt{\varepsilon_d} \sin(\theta) = \frac{2\pi}{\lambda} \sqrt{\varepsilon_d} \sin(\theta)$$
 (2)

Surface plasmon resonance (SPR) is the resonance between surface plasmons (SPs) waves and incident light waves. The mechanism of SPR can be explained by Equations (1) and (2) below [39]. This condition is achieved when the propagation constant of SPs (k_{sp}) iequals the propagation constant of the incident light (k_x) . Surface plasmons (SPs) are collective oscillations of electrons at the interface of thin-film metals such as gold (Au) and silver (Ag) with the dielectric due to the difference in refractive index at the interface. Equation (1) shows the relationship between propagation constant SPs (k_{sp}) and propagation constant incident light in a vacuum medium (k_0) , with ε_m and ε_d as the dielectric constant of metal and dielectric, respectively. Based on Equation (1), the k_{sp} is always higher than the propagation constant of directly injected incident light to the metal and dielectric interface [40, 41]. Various techniques have been developed to enhance k_x , including optical waveguide [42, 43], diffraction grating [44, 45], prism coupler [39, 46], and optical fiber. Through these approaches the k_x can be written as Equation (2). AFigure 1(b) shows that k_x is amplified and intersects with k_{sp} at a certain point, indicating surface plasmon excitation or SPR.

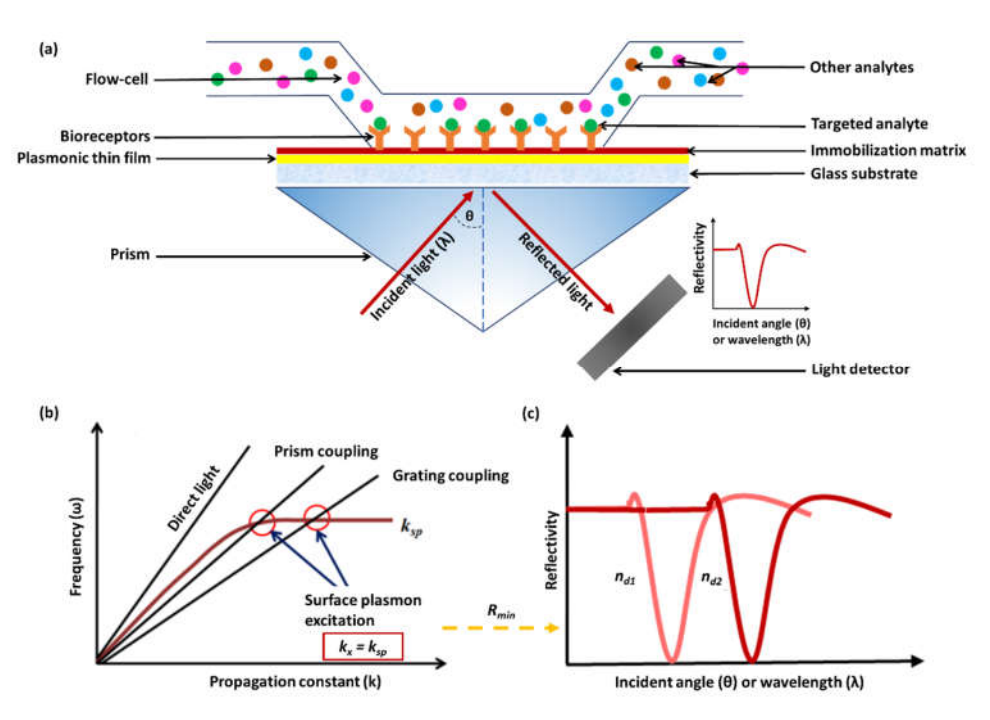


Figure 1 (a) Schematic of SPR components and detection principle; (b) The surface plasmon excitation possibilities by using incident light which directly injected and coupled. Reproduced with permission from ref [50]. Copyright 2016 MDPI; (c) The SPR curve and R_{min} shifted when the refractive index changes

Fiber optic-based SPR is an alternative SPR device that is more compact, flexible, low-cost, and suitable for remote sensing applications [51]. The smaller device size than prism-based SPR allows the integration into various microelectromechanical (MEMS) technologies such as microfluidic [52, 53]. Fiber optic-based SPR has the potential to be developed for chemical or biomolecular sensors in medical contexts. Fiber optic-based SPR is classified into two types based on the scattering mode, with the mechanism illustrated in Figure 2(a) [54]. The forward scattering mode measures the transmitter light, which is the excited SPs interacting with the SPR system in the center of the optical fiber. In comparison, the backward scattering mode places the sensing zone at the

end of the optical fiber. Hence, excited SPs are measured through the reflected light at the other end. Optical fibers can also be classified according to their design, including geometry-modified fibers and grating-assisted fibers [55]. Geometry-modified fibers removed the cladding to directly expose the sensing medium with coreguided light, such as unclad fiber, side-polished fiber, hetero core fiber, U-shaped fiber, and arrayed fiber (see Figure 2 (b)). Meanwhile, the grating-assisted fibers use grating to diffract the light into the cladding to reach a sensing medium. Designs that have been widely used for SPR sensor applications include long-period fiber gratings (LPFGs) and titled-fiber Bragg gratings (TFBGs) (see Figure 2(c)).

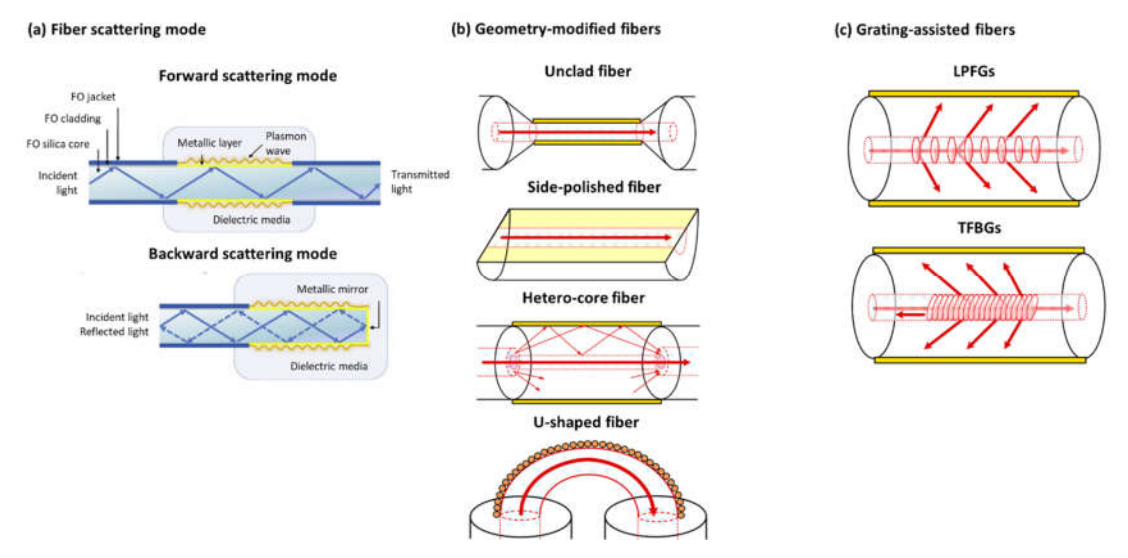


Figure 2 Different types of fiber optic-based sensors classified by (a) scattering mode and design included (b) geometry-modified fibers and (c) grating-assisted fibers. Reproduced with permission from ref [55]. Copyright 2015. Springer.

2D Materials Properties

Graphene

Graphene deserves to be called a pioneer and the most known 2D material since it was first fabricated by Novoselov et al. (2004) from the mechanical exfoliation of graphite [56]. The success of graphene in yields excellent properties, including its carrier mobility [57], thermal conductivity [58], mechanical strength [59], and optical transparency [60], attract research attention in various fields, especially electronics [61, 62] and optoelectronics [35, 63-65]. As illustrated in Figures 3(a) and (b), graphene is a two-dimensional form of carbon allotrope arranged in hexagonal lattice with sp^2 hybridization. Typically, the length of each carbon atom is 1.24 Å, and the distance between each layer is 3.4 Å. Graphene has a stable hexagonal structure owing to the formation of three strong σ bonds between each atom. Moreover, each atom donates one unpaired electron, forming a π bond, which is vertical to the graphene plane. The high conductivity of graphene is attributed to the presence of π bond that allows the electrons to move freely. A single layer of carbon atoms arranged in a hexagonal lattice structure with many π bonds formed by the noninteracting carbon atoms, which freely move between the layers [66, 67]. Therefore, graphene is suitable for immobilization matrix in sensor systems because it should increase the adsorption of biological molecules through π interaction due to its carbon-based structure [25].

Electronic properties. Graphene is generally known as a zero-bandgap semiconductor as a consequence of the identical environment of the two carbon atoms in the graphene unit cell [68, 69]. As mentioned earlier, the π electrons mainly contribute to its electronic properties. Each π electron hybridizes in forming π and π^* where the π -states and the π^* -states form valence and conduction bands, respectively. These two bands touch at six points, the so-called Dirac or neutrality points (see Figure 3(c)). Symmetry allows these six points to be reduced to a pair, K and K', which are independent. At low energy, one can observe the band structure with two cones touching at E_{Dirac} due to its linear dispersion [68]. The zro bandgaps in graphene can be opened using several

techniques, such as doping [70], chemical reactions to make different potentials between two atoms [71], or reducing the dimensionality to imitate particles in a narrow-long quantum box [72, 73]. Numerous sensor studies have exploited the tunable bandgap of graphene to provide suitable properties to detect specific targets [70, 74]. Graphene has exceptional transport properties where carrier density strongly affects the effectiveness of carrier movement in graphene [58, 75]. High carrier mobility in graphene allows better adsorption of molecules, which is beneficial for sensing devices like SPR sensors [76].

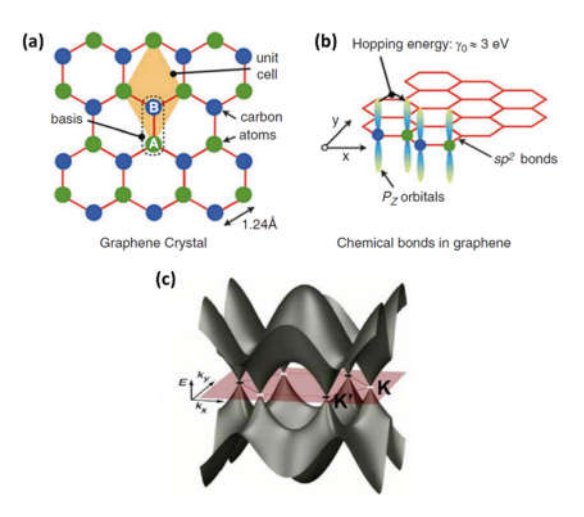


Figure 3 (a) The hexagonal crystal structure of graphene showing the atomic basis, the interatomic distance, and the unit cell; (b) The chemical bonds showing the sp^2 hexagonal structure with the P_z orbitals. Reproduced with permission from ref [77]. Copyright 2012 Springer; (c) The 3D bandstructure of graphene showing zero bandgaps. Reproduced with permission from ref [68]. Copyright 2010 American Chemical Society.

Optical properties. The optical properties of graphene were excellent and unique due to its zero bandgap characteristics. A monolayer of graphene can absorb the same amount of 1.55 μ m wavelength of light as the 20 nm thickness of InGaAs. The monolayer of graphene has been characterized as having 97% transmission, 2.3% of absorption, and <0.1% of reflection [68]. Moreover, the number of graphene layers determines the transmission, where the transmission tends to decrease as the number of layers increases [60]. The absorption capacity of graphene can be tuned by an external field or spintronic effects such as carrier spin-orbit coupling. The presence of an external field can be inhibited within a range of $2\Delta E_F$, where ΔE_F is the field-induced displacement of the Fermi level from the Dirac point [78]. Meanwhile, the spin-orbit coupling allows zero bandgap materials to absorb light properly. It can be enhanced by up to 100% in the terahertz frequency region, which was previously impossible due to the strict energy proportionality to k [79]. The combination of high transmission, high adsorption, and high conductivity of graphene makes it excellent for optical sensors such as fluorescence resonance energy transfer (FRET) and SPR.

Transition Metal Dichalcogenides (TMDCs)

2D TMDCs were discovered for the first time in 1963 by Robert Frindt using adhesive tape exfoliation methods [80]. Meanwhile, the suspension method first produced a monolayer of MoS₂ in 1986 [81]. Since then, the development of various nanostructures of MoS₂, such as nanotubes and nanoparticles, has continued along with the development of graphene study [82, 83]. The general formula of TMDCs is MX₂, where M is transition metal (group IV to VII), and X is chalcogen (S, Se, or Te). In multilayer and bulk samples, TMDCs are formed as stacked layers bound by a weak Van der Waals force. Therefore, the layers can be easily separated into individual layers consisting of three atomic planes (chalcogen-metal-chalcogen) with atomic thickness [84]. As shown in Figure 4(a), the different stacking orders of the atomic planes lead TMDCs to form different structures of hexagonal planar, including trigonal prismatic (2H) and octahedral (1T) coordination. The position of the chalcogen atom on each plane differentiates both structures. In the 2H structure, it occupies the same position (ABA).

Meanwhile, in the 1T structure, the chalcogen position was varied (ABC) [85]. TMDCs were categorized as a supermaterial after graphene because of their remarkable electronic and optical properties.

Electronic properties. The electronic properties of TMDCs are varied based on the chemical composition, structural phase, and thickness. The TMDCs in bulk are categorized as indirect bandgap materials with minimum conduction band at Q-points and maximum valence band at 1-points [86, 87]. The decrease in layer number gradually shifts the bandgap into direct type in a monolayer of TMDCs [30, 88]. In the case of MoS₂, when the number of layers decreased, the change in quantum confinement and hybridization between p_2 in s and d in Mo atoms give a strong interlayer coupling effect to the band at 1-points [34, 89]. Meanwhile, the direct bandgap, located at two inequivalent high-symmetry K- and K'-points, is relatively unaffected by the interlayer coupling [85-87]. Therefore, the direct bandgap is formed because of the unchanged band around K-points, while the indirect bandgap at 1-points significantly becomes larger. The indirect-direct bandgap transformation can be observed on all TMDCs materials as calculated by the first principal density functional theory (DFT). Figure 4(b shown the bulk and monolayer band of structure TMDCs, material including MoS₂ and WS₂ [31]. The direct bandgap in monolayer TMDCs significantly influences the performance in photonic, optoelectronic, and sensing applications.

Optical properties. The optical properties of TMDCs are also affected by the band structure previously described. TMDCs provide optical absorption over a wide wavelength range between the near-infrared and visible light regions [32, 33, 90]. The optical absorption, dominated by direct transition from conduction to the valence band, is identified as energy-independent joint-density-of-states and transition matrix elements near parabolic band edges [91]. The efficient optical absorption of TMDCs could enhance the detection signal in a opticals sensor such as SPR by 20-50% because it provides more excitation energy for efficient charge transfer [92-95]. In addition, the measurement resulted in a strong excitonic effect on the TMDCs material, which is indicated by a sharp resonance peak as shown by the solid line in Figure 4(c) [34, 89, 96]. The strong excitonic effect is in agreement with the theoretical calculation [97, 98] measurement from optical spectroscopy [99] and scanning tunneling spectroscopy [100], which confirm that TMDCs have large exciton binding energies around 0.4 - 1.0 eV [98, 100-105]. Large exciton binding energies increased light-matter interactions due to the strong excitonic oscillator, leading to a short radiative lifetime or significant radiative rate [88, 91]. Stronger light-matter interaction was advantageous for sensor application because it was considered an essential factor in improving the sensitivity [106].

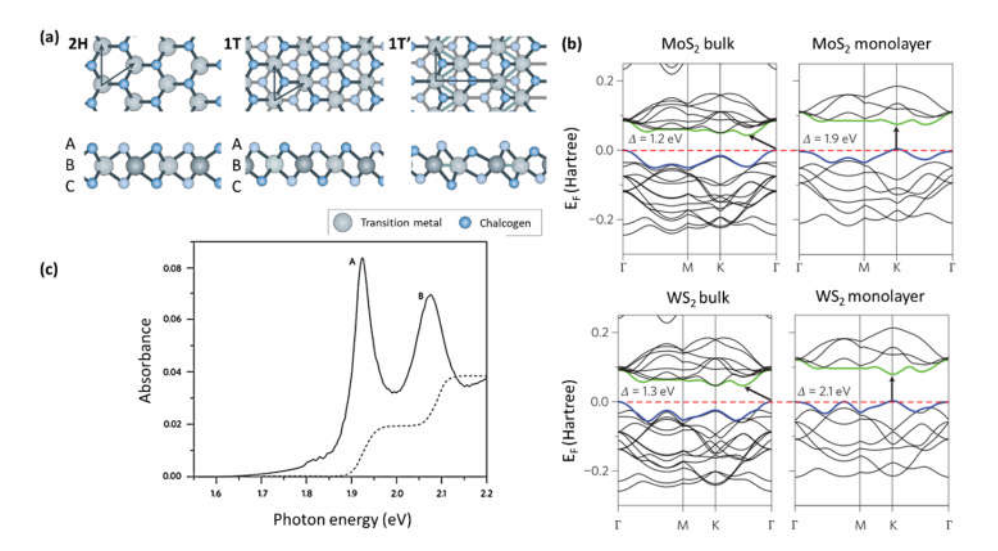


Figure 4 (a) Atomic structure of monolayer TMDCs with different atomic coordination. Reproduced with permission from ref [85]. Copyright 2017 Springer Nature; (b) Band structures calculated from first-principles density functional theory (DFT) for bulk and monolayer MoS₂ and WS₂ Reproduced with permission from ref [30]. Copyright 2012 Springer Nature (c) Absorption spectrum of monolayer MoS₂ at 10 K without excitonic effect (dashed line) and with excitonic effect (solid line). A and B are exciton resonances corresponding to transitions from the two spin-split valence bands to the conduction bands. Reproduced with permission from ref [88]. Copyright 2016 Springer Nature.

MXene

Transition metal carbides/nitrides/carbonitrides popular as MXene is one of the newest 2D materials developed by Naguib et al. in 2011 [107]. MXene is arranged by transition metal (M) and carbon or nitrogen (X) in the general formula of $M_{n+1}X_nT_x$ (n=1,2,3), with T_x representing the addition of surface groups. The surface group of T_x , such as -H, -F, -OH, or -O, remains as a byproduct from the etchants used in the synthesis process [108]. The numerous composition of MXene provides broad application such as desalination and water purification [109, 110], sensor [111, 112], energy storage [107, 113], and field effect transistor [114, 115]. Moreover, the abundant surface group allows more chemical and biomolecular binding and further functionalization, which is beneficial in sensor applications [116]. The structure of MXene crystal is hexagonal, closed-packed, and can be broken down into layered structures that form a sandwich structure with one layer of X atom located on octahedral interstitial sites between two layers of M atom. The M atom itself is arranged in close-packed arrays, as illustrated in Figure 5(a-f) [117, 118]. The ordering of M atoms was varied to maintain the stability of the structure in different crystal formulas of M_2X , M_3X_2 , and M_4X_3 [119, 120]. The 2D MXene can be obtained from layered MAX precursors via etching, the weak M-A bond can be chemically etched, while the M-X bond is withstood due to strong bonding [121].

Electronic properties. The theoretical calculation reveals that pristine MXene band structures show metallic behavior with Fermi energy found at the d bands of transition metal [122-124]. The semiconducting properties can be owned through some compositional modification and post-treatment, as reported in numerous studies [125]. The existence of surface group T_x shifts the Fermi energy to the gap between d bands of transition metal and p bands of carbides/nitrides. As a result, the MXene turns to be a semiconductor [124].

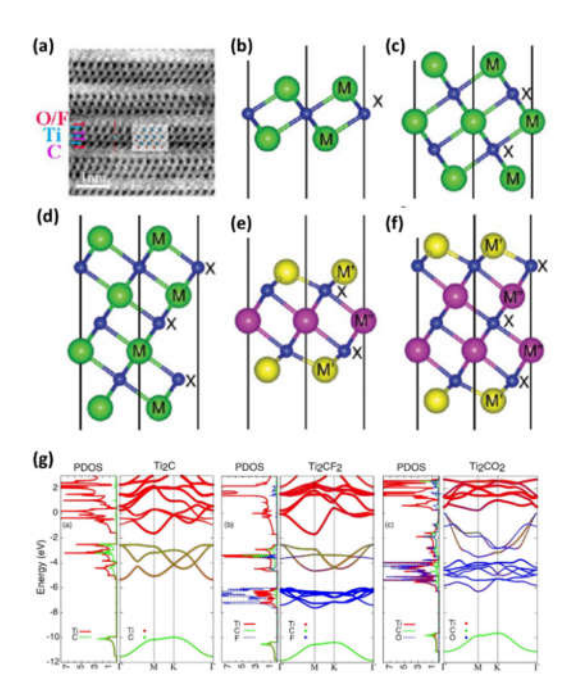


Figure 5 (a) Crystal structures of 2D MXenes high-angle annular bright-field image of Ti₃C₂T_x. Reproduced with permission from ref [118]. Copyright 2015 American Chemical Society; Side views of pristine (b) M₂X, (c) M₃X₂, (d) M₄X₃, (e) M₂'M"X₂, and (f) M₂'M₂"X₃ (g) Projected density of states [PDOS (states/eV/cell)] and projected band structures for Ti₂C, Ti₂CF₂, and Ti₂CO₂. The Fermi energy is located at zero energy. Reproduced with permission from ref [124]. Copyright 2017 Royal Chemical Society:

Figure 5(h) shows the band structure transformation from $M_{n+1}X_n$ to $M_{n+1}X_nT_x$ [124]. The bandgap can transform from the indirect to direct band through some treatments, including external field and mechanical treatment [126-129]. The bandgap changes from indirect to direct band were observed on Ti_2CO_2 , Zr_2CO_2 , and Hf_2CO_2 under biaxial strain of 4%, 10%, and 14%, respectively [129]. Besides bandgap transformation, the wide bandgap in Sc_2CO_2 MXene was also reported to decrease by the increment of tensile strain from 0 to 5% [128]. The tuning

of the bandgap in Sc₂CO₂ can also be performed by the change in the applied electric field, where the higher electric field resulted in the narrower bandgap [126, 127]. Easily tunable bandgaps of MXene enable these materials to attain desired properties for specific sensor applications.

Optical properties. Studies on the optical properties of MXene are still very limited. Several experimental studies reported the transmittance of thin film Ti₃C₂T_x, which possesses 70 − 90% transmittance [131, 132]. The highest transmittance was obtained by applying the intercalated species such as NH₃ and NH₄^{+,} which can increase transmittance three times compared to the MAX phase of Ti₃AlC₂ [130]. The increase in the thickness of MXene linearly improves the absorbance capability [131]. Berdiyorov et al. (2016) reported a theoretical study to reveal the effect of surface functionalization in $Ti_3C_2T_x$ on their optical properties. Generally, the static dielectric function of MXene is reduced by more than two times [133]. The oxygen termination contributes mainly to the total density of states near the MXene Fermi level [134]. Therefore, the calculation has found the more significant absorption provided by the sample with oxygen termination compared to hydroxylated/fluorinated termination. Consequently, the hydroxylated/fluorinated termination offers a better transmittance [133]. MXene can enhance the performance of SPR and other optical sensors through bulk plasmonic behaviors. Interestingly, the plasmonic properties of MXene differ from most plasmonic materials that depend on the number of layers. The MXene is not strictly required to be a single layer to obtain the bulk plasmonic phenomenon and applied in the plasmonic system [135]. Considering limited cheap and precise monolayer fabrication techniques, MXene becomes a good alternative to obtain excellent absorption and plasmonic properties from a low-cost technique like the aqueous acid technique [136].

SPR Sensor using 2D Materials

Graphene-based SPR Sensor

SPR sensor is a convenient technique to exploit the electronic and optical properties of graphene. The excellent properties of graphene and the advantages of SPR can complete the puzzle in developing excellent performance, reliability, and procedure/cost-effective sensor technology. Graphene has surface characteristics that enhance the efficient adsorption of chemical and biological molecules due to its high surface-to-volume ratio, high carrier mobility, and carbon-based structure, enabling π stacking interaction [25, 76]. High optical absorption of graphene could provide more energy transferred to the sensing system, thereby improving the sensing signal [68, 95, 137]. Moreover, graphene also acts as a protective layer to prevent metallic layers from oxidation and degradation [25]. In general, graphene is utilized as an immobilization matrix on the SPR chip, either as bare graphene and its derivatives or in combination with other materials [138, 143]. The simulation approach has been used to optimize the number of layers and thickness of graphene to produce the optimum enhancement. The efficiency of the finite element analysis (FEA) method and transfer matrix method (TMM) for the N-layer system have been compared to investigate the optimum thickness of graphene. Both methods have shown an acceptable result of the SPR curve [144]. The TMM is used for analytical preliminary study. Therefore, this method was limited in simulating the structure and roughness of the SPR surface [145]. Meanwhile, the FEA method, which can be carried out using specific software such as COMSOL Multiphysics and Finite-difference time-domain (FDTD) Lumerical, is more beneficial because it can simulate various materials with various structures of geometry also provides information about electromagnetic behaviors on the design [144]. Bhavsar et al. (2015) have reported each monolayer graphene on the SPR surface absorbs 2.3% of light [146]. As shown in Figure 6(a), increasing the layer increases angular dip shifting, indicating a sensitivity enhancement. However, the broadening of the SPR curve is a matter of concern due to wider FWHM causing the angular shifting to be challengingt to observe, it also decreases the quality factor and detection accuracy [147]. The broader curve is caused by the high extinction coefficient of graphene that causes the shift of wave vectors of surface plasmons to meet the conditions of surface plasmons [148].

Meshginqam et al. (2017) reported the sensitivity of graphene-based SPR sensors to analyze the single-stranded DNA (ss-DNA) hybridization during double-stranded DNA (ds-DNA) formation. The modification resulted in an enhancement of up to 32% compared to bare Au, where a maximum sensitivity of 120 deg/RIU was obtained for a 6 nm thickness of graphene. The increase in sensitivity is shown by a graphene layer of less than 10 nm. Increasing the thickness was found to cause the sensitivity to be decreased significantly due to the limitation of

optical absorption [144]. Pandas et al. (2020) conducted a similar study and reported the optimum monolayer graphene thickness of 0.34 nm. The monolayer graphene was applied in SPR simulation to detect glucose with a measured sensitivity of 272.15 deg/RIU [147]. Pseudomonas sensor measurements were carried out preliminarily using the N-layer method, showing that the sensor provides a sensitivity of 33.98 degrees/RIU and a quality factor of 2.78019. The simulated thicknesses of graphene are 10 and 20 layers, showing the SPR curve, which is very broad and shallow. The FWHM and reflectivity are $^{\sim}20$ degrees and 0.30 - 0.75, respectively. However, this curve is no longer acceptable for analyzing SPR sensor performance [145]. Therefore, the used thickness of graphene in SPR sensors is recommended to be less than ten layers.

Using an experimental approach, Chung et al. (2018) reported that SPR with monolayer and doubled layers of graphene on exposure to streptavidin reached a sensitivity of 171.33 deg/RIU and 179.79 deg/RIU, respectively. This sensitivity is $^{\sim}3.7$ times higher than that of direct immobilization of streptavidin on bare Au, which is a satisfactory result [138]. A graphene layer applied to a positively charged Au film was used to detect -thrombin aptamer (TBA). For 100 ng/cm of TBA coverage on the sensing surface, the SPR curve was shifted by 120 mDeg [149]. Since graphene has a high electric field around the surface, the analyte absorption and sensor performance are improved [147]. Layer-by-layer graphene can be prepared using the chemical vapor deposition (CVD) method and measured using an SPR angular scan to monitor the number of layers. Each monolayer graphene shifts the SPR curve by $0.46 \pm 0.07^{\circ}$, and as previously mentioned, the widening of the curve is shown as the number of layers increases [138].

The derivatives and modified derivatives of graphene, such as graphene oxide (GO), reduced graphene oxides (rGO), carboxyl-functionalized GO (cGO), and nitrogen-doped rGO (N-rGO), have attracted much attention in the development of SPR sensors. GO has abundant oxygen functional groups that are suitable for immobilizing various biomolecules via covalent, non-covalent, and electrostatic bonds [150]. Since GO is a single layer of graphite, GO can be prepared using Hummer's and Offeman's methods from the graphite powders [151]. From the FEA simulation methods, GO has shown significant increases in binding sites compared to conventional graphene. By providing ~3.5 times more binding sites, the detection sensitivity of ds-DNA is increased by 23% compared to bare Au performance [144]. Wu et al. (2016) reported the response of a GO-based SPR sensor to pig IgG in the range of 1.25 – 40 μg/mL shifted the resonance wavelength to 0.20 – 3.20 nm. Meanwhile, cGO resulteshifted 0 – 5.80 nm in the range of 0.60 – 40 μg/mL. As shown in Figure 6(b), the cGO shows a better result due to the more binding sites of protein available, maintaining the optical performance of GO [152]. Other modified derivatives of graphene reported by Chung et al. (2018) compare rGO and N-rGO in biotin detection, resulting in a sensitivity of 128.91 deg/RIU and 130.01 deg/RIU, respectively [138]. The rGO application in SPR sensor has been investigated for E. coli detection, it was shown that minimal π - π stacking interactions were found in bacterial adhesion to rGO. In addition, the electrostatic interaction is predominated during the adsorption. [153]. It can be seen in Figure 6(c) that the rGO is not as significant as graphene in improving conventional SPR sensor performance.

The modification of graphene has also been involved in other materials for amplifying response signals or providing more binding sites. Gold nanoparticles (AuNPs) are attractive materials because they provide both features. Gold nanorods (AuNRs) is known to be very sensitive to changes in environmental condition due to their longitudinal mode of plasmon resonance wavelength [154]. The GO modification with AuNRs is advantageous because it has a high loading capacity from graphene and excellent optical properties from Au [155]. The AuNRs were applied to the GO surface and modified by the rabbit anti-transferrin using EDC/NHS linking chemistry. The sensitivity of the SPR sensor was enhanced by $^{\sim}4$ times compared to bare Au. The sensor also reached the limit of detection (LOD) of 0.0375 µg/mL. The selectivity feature was shown when the sensor was exposed to the bovine IgG and human IgG, whereas the shifting was not observed, which indicates specificity of detection [155]. Graphene as a 2-dimensional material that possesses various functional group str, strongly supports the extraction efficiency of biomolecules per unit area [156]. The optical properties of SPR were also amplified by the AuNRs presence due to its localized surface plasmon [155]. Other types of AuNPs which are gold nanostars (AuNSs) also has been reported to enhance the cGO-based SPR sensor [152]. The AuNSs were synthesized through surfactant-free methods to obtain accessible sites for directly binding analyte molecules [157]. The AuNSs have thorn-like shells that produce a better local electromagnetic field than AuNPs, as well as resonant shifting, which enhances up to 200% and reaches 0.0375 $\mu g/mL$ of LOD in the detection of pig IgG. The

selectivity of the sensor was also observed, as shown in Figure 6(d) whereas the wavelength shifting against pig IgG is significantly higher than a response to human and bovine IgG [152].

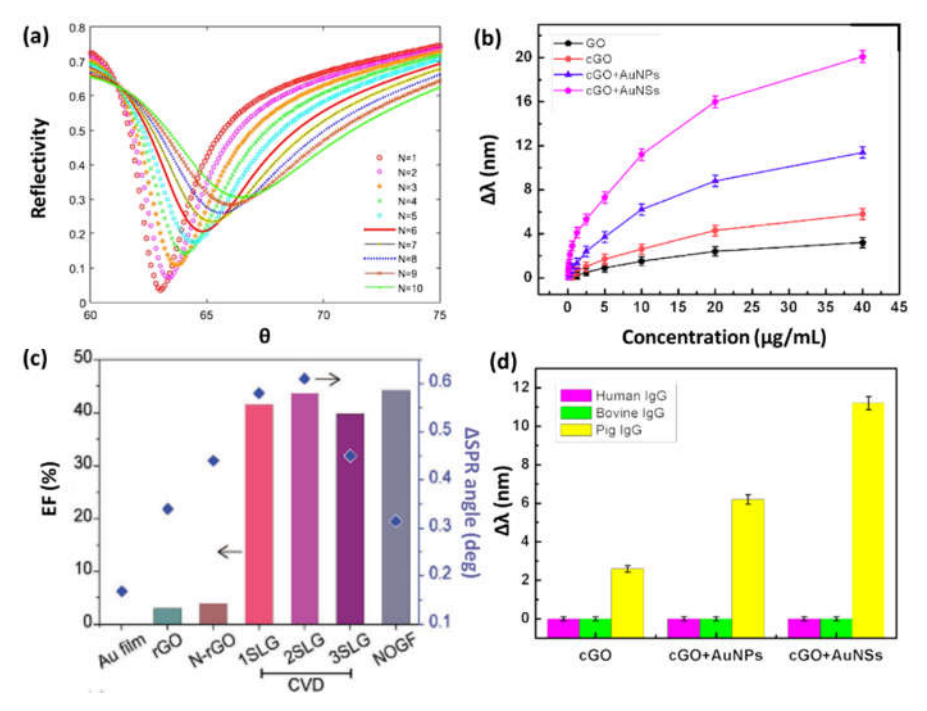


Figure 6 (a) SPR curve for different number of graphene layers. Reproduced with permission from ref [144]. Copyright 2017 Springer Nature; (b) Relationships between concentrations of pig IgG and shifts of resonant wavelengths obtained with biosensors based on GO, cGO, cGO/AuNPs-antigen and cGO/AuNSs-antigen conjugate Reproduced with permission from ref [152]. Copyright 2016 Elsevier; (c) Enhancement factor and streptavidin sensing results from different samples of derivatives graphene. Reproduced with permission from ref [138]. Copyright 2018 Wiley; (d) The selectivity shown by the shifts of resonant wavelengths obtained for different antigens by using SPR biosensors based on cGO, cGO/AuNPs and cGO/AuNSs sensor chip. Reproduced with permission from ref [152]. Copyright 2016 Elsevier

Besides Au, various materials have also been investigated to improve graphene-based SPR sensors, such as other types of 2D materials [140, 141, 158, 159] and polymer [160-163]. Modifications by polymer were performed by building the polymer-graphene composites or layer-by-layer structure. Hu et al. (2014) reported the polydopamine (PDA)-rGO composites for the detection of carcinoembryonic antigen (CEA) by the SPR imaging (SPRi) platform [160]. PDA is reactive to several chemical groups, such as thiols and amine. Therefore, this material was considered to improve the active sites in graphene-based SPRi [164]. The sensors resulted in an LOD of 50 ng/mL without amplification and enhanced to 0.5 ng/mL in dual signal amplification, which indicates excellent sensitivity and reliability for human serum measurement [160]. Sadrolhosseini et al. (2021) used polypyrrole (PPy) to modify the GQDs for the SPR immobilization layer [161]. The PPy-GQDs composited was produced by electrochemical polymerization. This composite has been studied for detection in various techniques [165-167]. The sensors can detect the presence of arsenic, mercury, and lead with LOD 0.005 ppm, with the highest sensitivity obtained in arsenic detection [161]. In another study, nitrilotriacetic acid (NTA) was included in the polymerization process. Thus, PPy-NTA is obtained, which is then applied on the graphene surface. The PPy-NTA-modified SPR was used for anti-cholera toxin (anti-CT) detection and has shown excellent LOD of 4 pg/mL. A different technique of polymer-based modification was reported by Primo et al. (2018), the poly(diallyldimethyl)ammonium (PDDA) was included in Au/MSA/PDDA/GO wafers [163]. The biosensor was performed to detect Galectin-3 (Gal3), resulting in LOD 2 ng/mL. The sensorgram indicates the selectivity of the sensor to Gal3 compared to transferrin, human serum albumin (HSA), hemoglobin, and IgG detection [163]. In another study, the graphene-based SPR combined with the perovskite oxide, strontium titanate (SrTiO₃), in the hybrid structure of Ag/STO/graphene. This structure results in high sensitivity in several types of malaria detection ranging between 278 - 400 deg/RIU [168].

Table 1. Summary of studies related to graphene based SPR sensors and its performance enhancement

s the density of streptavidin s 3.6 times shifting ad to bare Au sence of an active layer sence of an active layer s the changes in refractive jacent to the Au surface on ability of graphene to cules armal sensitivity, i.e., the of refractive index with ture is extremely small sitivity was increased by sitivity enhancement make layer of graphene s 2.3% light absorption sitivity enhancement than sitivity enhancement than a 3.25 times higher the of binding sites sitivity was increased by ensity near the graphene terface is around twice, eleading to the ment absorption of	Hybrid Structure	Methods	Bioreceptors	Analytes	Enhancement Mechanism	Performance	Ref.
deposition and albumin evolution and albumin evolution method Wet process and spin - Co²+ The presence of an active layer coating coating and spin - Co²+ The presence of an active layer increases the changes in refractive index adjacent to the Ausurface index adjacent ansity in transfer matrix methods Simulation using finite - Ss-DNA and 3.2% sensitivity was increased by transfer matrix method and simulation using finite - Ss-DNA and 3.2% sensitivity enhancement than element analysis (FEA) and ss-DNA and an adjacent analysis (FEA) and and a simulation using finite - Simulation using finite - Ss-DNA and a signer and analysis (FEA) and analysis (FEA) analys	Au/graphene 2 SLG			Bovine serum	 Increases the density of streptavidin 	S = 179 deg/RIU	[138]
Wet process and spin - Co2+ Wet process and spin - Co2+ Coating Simulation using Frobe DNA Ss-DNA and Simulation using finite - Simulation using method Simulation				albumin	 Increases 3.6 times shifting 		
Wet process and spin - Co²+ • The presence of an active layer increases the changes in refractive increases the changes in refractive increases the changes in refractive index adjacent to the Au surface biomolacules are transfer matrix methods Isimulation using finite - Simulation using finite - Simulation using finite - Simulation using method - Simulation - Simulation using method - Simulation - Simulation using method - Simulation - Simula		exfoliation method		(BSA)	compared to bare Au		
increases the changes in refractive index adjacent to the Au surface Simulation using Probe DNA ss-DNA and simulation using finite - Simulation using finite - Simulation using Nicotine Blood wattransfer matrix methods Simulation using Book and simulation using Final F	Au/chitosan-GO/CdS	l	- (Co ²⁺	 The presence of an active layer 	S = 0.1188 deg/ppm	[139]
Simulation using Probe DNA ss-DNA biomolecules • Low thermal sensitivity, i.e., the change of refractive index with temperature is extremely small transfer matrix methods From Simulation using finite - ss-DNA and simulation using sites Simulation using nicotine pseudomona and the sensitivity was increased by simulation using - leield intensity near the graphene and transfer matrix methods Simulation using - selike and single layer interface is around twice, therefore leading to the enhancement absorption of analytes	QDs solution				increases the changes in refractive index adjacent to the Au surface		
transfer matrix methods Simulation using finite - Simulation using -	Au/WS ₂ /graphene			ss-DNA	 Absorption ability of graphene to 	S = 95.71 deg/RIU	[140]
• Low thermal sensitivity, i.e., the change of refractive index with temperature is extremely small simulation using finite - ss-DNA and element analysis (FEA) arethod ss-DNA and element analysis (FEA) arethod ss-DNA and element analysis (FEA) arethod ss-DNA are lement analysis (FEA) arethod are simulation using finite - ss-DNA are sensitivity enhancement than bare Au method are simulation using niction are sendomona are sensitivity was increased by MATLAB are sensitivity was increased by solid are sensitivity was increased by solid are sensitivity are the graphene glucose leading to the enhancement absorption of analytes		transfer matrix method			biomolecules		
Simulation using Probe DNA ss-DNA • The sensitivity was increased by transfer matrix methods Element analysis (FEA)					 Low thermal sensitivity, i.e., the 		
Simulation using Probe DNA ss-DNA and element analysis (FEA) ss-DNA element analysis (FEA) ss-DNA element analysis (FEA) ss-DNA element analysis (FEA) ss-DNA element analysis (FEA) element analysi					change of refractive index with		
Simulation using finite - ss-DNA and such sample analysis (FA) - ss-DNA and such sample analysis (FA) - ss-DNA and such single layer of graphene increases 2.3% light absorption simulation using finite - ss-DNA such semsitivity enhancement than element analysis (FA) - ss-DNA such semsitivity enhancement than element analysis (FA) - ss-DNA such sensitivity enhancement than element analysis (FA) - ss-DNA such sensitivity enhancement than element analysis (FA) - such sensitivity enhancement than element analysis (FA) - such sensitivity enhancement than element analysis (FA) - such sensitivity was increased by MATLAB - such sensitivity was increased by such sensitivity mear the graphene glucose layer interface is around twice, therefore leading to the enhancement absorption of analytes					temperature is extremely small		
transfer matrix methods ten Simulation using finite - ss-DNA and e 32% sensitivity enhancement ds-DNA increases 2.3% light absorption Simulation using finite - ss-DNA e Each single layer of graphene increases 2.3% light absorption Simulation using finite - ss-DNA e 23% sensitivity enhancement than bare Au bare Au bare Au enthod Simulation using Nicotine Pseudomona e The sensitivity was increased by s-like bacteria Simulation using - Blood e Field intensity near the graphene glucose transfer matrix methods Each single layer of graphene increases 2.3% light absorption of analytes	Au/MoS ₂ /graphene			ss-DNA	 The sensitivity was increased by 	S = 89.29 deg/RIU	[141]
ten Simulation using finite - ss-DNA and • 32% sensitivity enhancement ds-DNA each single layer of graphene increases 2.3% light absorption simulation using finite - ss-DNA ss-DNA sandlytes EA simulation using finite ss-DNA sandlytes Each single layer of graphene increases 2.3% light absorption ss-DNA sandlytes sandlyt		transfer matrix method	,		~53%		
element analysis (FEA) Simulation using finite - Simulation using finite - Simulation using notion using notion using remarks the method Simulation using Nicotine Pseudomona - The sensitivity was increased by selike bacteria Simulation using - Simulation using		Simulation using	- 0		 32% sensitivity enhancement 	S = 120 deg/RIU	[144]
Simulation using finite - ss-DNA • 23% sensitivity enhancement than element analysis (FEA) • Provide 3.25 times higher the number of binding sites Simulation using Nicotine Pseudomona • The sensitivity was increased by s-like bacteria Simulation using - Blood • Field intensity near the graphene glucose transfer matrix methods glucose enhancement absorption of analytes	layers			ds-DNA	 Each single layer of graphene 		
Simulation using finite - ss-DNA • 23% sensitivity enhancement than bare Au method Simulation using Nicotine Pseudomona • The sensitivity was increased by s-like bacteria Simulation using - Blood • Field intensity near the graphene glucose transfer matrix methods glucose enhancement absorption of analytes		method			increases 2.3% light absorption		
element analysis (FEA) method Simulation Using Nicotine Simulation Simulation Using Simulation Simulation Simulation Using Simulation	Au/G0		- 0	ss-DNA	 23% sensitivity enhancement than 		[144]
method Simulation using Nicotine Pseudomona The sensitivity was increased by s-like bacteria Simulation using Blood Field intensity near the graphene glucose transfer matrix methods glucose leading to the enhancement absorption of analytes					bare Au		
Simulation using Nicotine Pseudomona The sensitivity was increased by AATLAB Simulation using Blood Field intensity near the graphene glucose transfer matrix methods glucose leading to the enhancement absorption of analytes		method			 Provide 3.25 times higher the 		
Simulation using Nicotine Pseudomona • The sensitivity was increased by s-like ~10% Bacteria Simulation using - Blood • Field intensity near the graphene glucose transfer matrix methods glucose layer interface is around twice, therefore leading to the enhancement absorption of analytes					number of binding sites		
Simulation using - Blood • Field intensity near the graphene glucose transfer matrix methods glucose therefore leading to the enhancement absorption of analytes	Au/graphene			Pseudomona	 The sensitivity was increased by 	S = 33.97 deg/RIU	[145]
Simulation using - Blood • Field intensity near the graphene transfer matrix methods glucose layer interface is around twice, therefore leading to the enhancement absorption of analytes		MATLAB		s-like	~10%		
Simulation using - Blood • Field intensity near the graphene transfer matrix methods glucose layer interface is around twice, therefore leading to the enhancement absorption of analytes				bacteria			
transfer matrix methods glucose layer interface is around tw therefore leading to enhancement absorption analytes	Au/graphene	Simulation using	- 50	Blood	 Field intensity near the graphene 	S = 272.15 deg/RIU	[147]
leading to absorption	monolayer	transfer matrix method		glucose	layer interface is around twice,		
absorption					leading to		
analytes					absorption		
non-limin					analytes		

Table 1 Continued. Summary of studies related to graphene-based SPR sensors and its performance enhancement

Hybrid Structure	Methods	Bioreceptors	Analytes	Enhancement Mechanism Pe	Performance	Ref.
Au/graphene	ı	α -thrombin	α -thrombin	 TBA is adsorbed onto the graphene LC 	LOD = 0.05 nM	[149]
		aptamer (TBA)		layer through the strong noncovalent binding of graphene with nucleo-based		
Au/cGO/AuNSs	Hummers Offeman's method/	Rabbit anti-pig IgG	Pig lgG	immobilization y increasing the roups and retains GO for optical cules	LOD = 0.0375 µg/mL	[152]
Au/rGO/PSS	Modified Hummer's method and electrophoretic deposition	1	E. coli 107/86	efficient ules due to actions	LOD = 100 cfu/mL	[153]
Au/GO/AuNRs	Hummer's and Offeman's method	Rabbit anti- transferrin	Transferrin	 The shifting increase ~5x compared LOD = 0.0375 μg/mL to Au film sensor GO provides the highest extraction efficiencies of biomolecules per unit area of virtually any material 	DD = 0.0375 μg/mL	[155]
Au/BP/Graphene	Simulation using the transfer matrix method	Probe DNA	DNA	 The sensitivity was enhanced by S= ~57% Graphene enhances the physical adsorption of target ssDNA with probe DNA due to strong π stacking forces between target analyte, i.e., ssDNA and graphene surface 	S = 125 deg/RIU	[159]
Au/PDA-rGO	Hummer's method and oxidative polymerization	Anti-CEA antibody	CEA	PDA-functionalization of reduced LC GO nanosheets to improve the performance of SPR immunoassay significantly	LOD = 0.5 ng/mL	[160]

Table 1 Continued. Summary of studies related to graphene-based SPR sensors and its performance enhancement

Au/PPv-GQDs				Enhan	Ennancement Mechanism		o lo li la li co	-
	Electrochemical	-	Arsenic,	• The	enhancement	mechanism	mechanism LOD = 0.005 ppm	[161]
	polymerization		mercury, and	bas	based on the potent of electron	of electron		
			lead	trai	transport between GQDs and	GQDs and		
				ane	analyte ions			
Au/graphene/pyrene-	Chemical vapor	vapor Biotinylated	Anti-cholera	• Wo	• Monolayer graphene was exploited LOD = 4.0 pg/mL	s exploited	LOD = 4.0 pg/mL	[162]
NTA	deposition	cholera toxin (b- toxin from	toxin from	to	to amplify the SPR signals for	signals for		
		CT)	rabbit (anti-	chc	cholera, increasing the SPR sensor	SPR sensor		
			(L)	per	performances by 80% compared to	ompared to		
				the	the graphene-devoid setup	dn		
Au/MPS/PDDA/GO	Wet process deposition	anti-Gal3	Gal-3	• 60	GO role as antibody anchor point $LOD = 2.0 \text{ ng/mL}$	ichor point	LOD = 2.0 ng/mL	[163]
				anc	and amplifier of SPR response	onse		
Ag/SrTiO ₃ /graphene	Simulation using		Malaria	• Gra	aphene increases the	e absorbed	• Graphene increases the absorbed $S = 278 - 400 \text{ deg/RIU}$ [168]	[168]
	transfer matrix methods			light	ıt			
Au/CTAB/HGQDs	1	ı	Fe ³⁺	• The	The positive charge from Fe^{3+} and $S = 29.88 \text{ deg/ppm}$	m Fe³+ and	S = 29.88 deg/ppm	[169]
				ne£	negative charge from HGQDs form a LOD = 66.165 nM	QDs form a	LOD = 66.165 nM	
				sha	shared electron, resulting in strong	ng in strong		
				im	immobilization			

TMDCs-based SPR Sensor

TMDCs have been gaining tremendous attention among other alternative 2D materials. TMDCs offer wide bandgap, high optical absorption, and high surface-to-volume ratio that are suitable for optical sensors such as SPR [85, 88, 170]. High optical absorption in TMDCs resulted from the direct bandgap, enabling direct transition from conduction to the valence band [91]. As a result, more energy is transferred to the metallic layer interface to excite the surface plasmon and enhance the SPR response [95]. On the large surface of TMDCs, the more molecular target was absorbed and interacted with light efficiently due to a strong excitonic effect [88, 106]. The studies concerning TMDCs-based SPR sensors have been widely explored using a numerical/simulation approach or experiment. In the studies found in the last decades, simulations on TMDCs-based SPR have focused on their combination with other materials such as silicon, blue phosphorus (BlueP), and other 2D materials. Due to limitations of compositional and structural materials arrangement, the simulation commonly focuses on optimizing thickness using TMM or FEA methods.

Wang et al. (2017) use TMM to theoretically design the SPR sensor based on WS₂/graphene hybrid nanostructure [171]. Firstly, the WS₂, MoS₂, and graphene compared each other to obtain the best sensitivity. As shown in Figure 7(a), the resonance angle shifting of graphene is relatively lower than WS2 and MoS2, but when compared to bare Ag/Au sensors sensitivity (151.5 deg/RIU), the sensitivities of WS2, MoS2, and graphene are relatively higher which are 157.7 deg/RIU, 170.0 deg/RIU, and 177.5 deg/RIU, respectively. Further, the study on reflectivity at resonance angle for each 2D material was carried out. The results concluded that monolayer WS2 is the best 2D material due to minimum reflectivity, which indicates more efficient light absorption [171]. A higher sensitivity of 182.5 deg/RIU was obtained when graphene was deposited on the top of WS2 [171]; graphene is advantageous for selective detection because of its active sites [29]. Meanwhile, the different hybrid structures of graphene/WS2 on the Ag surface provided a significantly high sensitivity of 336 deg/RIU with a monolayer of graphene and 15 layers of WS2 [172]. The TMM analysis was also performed to simulate the sensitivity of hybrid MoS₂/graphene-based SPR sensors to detect DNA molecules. The sensitivity increases from 80.7 deg/RIU to 89.29 deg/RIU with two layers of MoS₂ stacked over the monolayer graphene [141]. Using Ag thin films, MoSe₂/graphene hybrid successfully performed high sensitivity for the detection of glucose in urine with concentration in the range of 0.015 - 10 g/dL. The sensitivity was found to be 215.5 deg/RIU, which is 2.42 times higher than that of bare Ag and 2.35 times higher than that of graphene-based sensors [173]. Different from graphene, TMDCs still performed sensitivity enhancement even when the number of layers is more than

Silicon has also been used to improve the performance of TMDCs-based SPR sensors because of its high refractive index and behavior as a protective layer for sensor systems [40, 174, 175]. Ouyang et al. (2016) performed the TMM and Fresnel equations to investigate the performance of silicone/TMDCs hybrid systems using various materials, including MoS2, MoSe2, WS2, and WSe2, to detect the change of refractive index (RI). Each hybrid structure showed better sensitivity compared to conventional SPR sensors with a sensitivity of 131.70 deg/RIU, 131.68 deg/RIU, 155.68 deg/RIU, and 141.40 deg/RIU, respectively [176]. The optimal TMDC layer is about 1-2 layers with 7 nm silicon thickness and 35-40 nm Au thickness; this combination of optimized thickness parameters is essential to minimize reflection and energy loss to achieve higher sensitivity [176]. The comparison between TMDCs materials was also obtained from the Au/TMDCs/Au/MXene structure. The MoS₂, MoSe₂, WS₂, and WSe₂ resulted in a sensitivity of 174 deg/RIU, 176 deg/RIU, 198 deg/RIU, and 192 deg/RIU, respectively. Similar to Ouyang et al. (2016), a structure with a WS2-based SPR sensor shows a higher sensitivity, which is an increase of 41.43% compared to a conventional SPR structure [177]. The use of BlueP-MoS₂ composite provided a significant improvement of SPR sensitivity, with the Kretschmann structure of CaF₂/ZnO/Au/BlueP-MoS₂, the sensitivity of 235 deg/RIU was obtained. The ZnO was applied to adhere to Au thin film, and the layers of BlueP-MoS2 were utilized to increase light interaction and decrease oxidation on the sensing surface [106].

Finally, the numerical analysis brings out WS $_2$ as the best TMDCs material among others [170, 174, 175]. However, the experimental studies commonly used the MoS $_2$ in the SPR sensors fabrication. 2D TMDCs can be prepared using various methods, including chemical vapor deposition (CVD) [178-180], atomic layer deposition (ALD) [181-183], exfoliation process [184-186], and hydrothermal methods [26, 187, 188]. The CVD technique has successfully fabricated a monolayer MoS $_2$ on the silver thin films, which functioned as a protective layer and

immobilization matrix for the anti-IgG. The SPR signals stability was checked by immersing the sensors in water for several hours, the SPR signals are broadened along with the oxidation of silver, which can be observed in Figure 7(b). Meanwhile, as shown in Figure 7(c) and (d), the SPR signals become more stable and more sensitive by shifting 0.5 degrees further with the application of monolayer MoS₂ [189]. Using a simple drop-casting method, the MoS₂ was deposited on the Au surface with a thickness of around 402.5 – 925.3 nm. The MoS₂modified sensors increased the sensitivity by 30.67% compared to bare Au sensors, the sensitivity of 2793.5 nm/RIU was reached in the deposition of 2 cycles MoS₂ [92]. Zhao et al. (2020) reported a more detailed experimental study of MoS₂ nanoflower-AuNPs-based SPR sensors, including material synthesis, sensor fabrication, and sensing measurements [26]. The hydrothermal methods have been reported in many studies to produce various MoS₂ nanostructures, including nanoflower [188, 190, 191]. The synthesis used ammonium molybdate tetrahydrate [(NH₄)₆Mo₇O₂₄·4H₂O] and thiourea [[SC(NH₂)₂] as molybdenum and sulfur precursors, respectively. The as-prepared MoS2 nanoflower powders were deposited on the Au film, followed by AuNPs deposition using the drop-casting method, the detailed process was shown in Figure 8(a). Under the exposure of bulk RI, the sensor showed a sensitivity of 2857.2 nm/RIU and 2149.7 nm/RIU for AuNPs-unmodified and modified sensors, respectively. In contrast, the higher sensitivity of mouse IgG detection is obtained from AuNPsmodified sensor with a comparison of 0.016 nm/(μg/mL) and 0.0472 nm/(μg/mL), respectively [26]. Since the TMDCs lack active sites, unlike graphene, the functionalization of AuNPs provides an ideal platform for antibody immobilization, making AuNPs-modified sensors more sensitive in immunoassay [192].

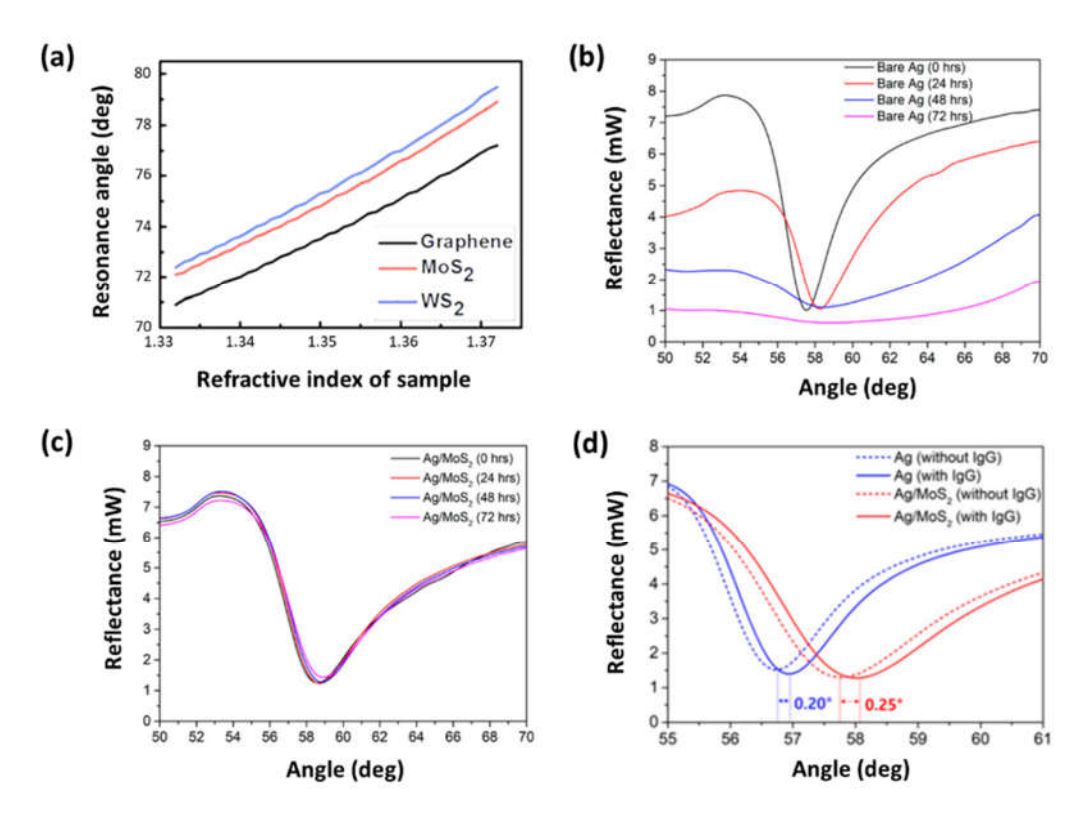


Figure 7 (a) Resonance angle shifting respect to the refractive index changes of sensors based on bimetallic film with graphene, MoS₂ or WS₂ film. Reproduced with permission from ref [171]. Copyright 2017 Royal Chemical Society; SPR signals stability of (b) bare Ag and (c) Ag/MoS₂ substrates in water for several hours; (d) SPR angle shift before and after the binding reaction of IgG of Ag substrate is 0.20 deg and that of the Ag/MoS₂ substrate is 0.25 deg. Reproduced with permission from ref [189]. Copyright 2019 MDPI.

Fiber-based SPR sensor has also used MoS_2 to optimize its performance in Bulk refractive index with a sensitivity of 3061 nm/RIU [93] and in E. coli detection, which achieved the LOD of 94 CFU/mL [193]. The MoS_2 can result from liquid exfoliation and deposited on the Au surface by dip coating technique [193]. $MoSe_2$ -modified fiber sensors also have a high sensitivity of 2821.81 nm/RIU and LOD of 0.33 μ g/mL in detecting goat-anti rabbit IgG

[37]. The higher performance was obtained from 5 cycles-deposited MoSe₂, the influences of deposition cycles on the sensor sensitivity are shown in Figure 8(b) [37]. In the study of Song et al. (2020), the MoS₂ was applied between the U-shaped fiber and Au thin film by electrostatic self-assembly [94]. The sensitivity of human IgG detection by proposed sensors was unexpectedly higher than a sensor with MoS₂ on the metal film, which is 6184.4 nm/RIU and 4946.8 nm/RIU, respectively. In the U-shape fiber configuration, the energy sources from the cladding mode light, which does not meet the total reflection condition, are transmitted to the surrounding medium. In the absence of MoS₂, light transmitted from the fiber to Au film is relatively low. The high optical absorption of MoS₂ provides sufficient light energy to generate the SPR phenomenon [94, 195]. Using the various analytes, including IgA, IgD, IgE, and IgG, the sensor coated with anti-IgG has excellent selectivity, where the wavelength shift for IgG reaches 22.3 nm, while for other analytes, it is only in the range of 0.21 - 0.45 nm (see Figure 8(c)) [94].

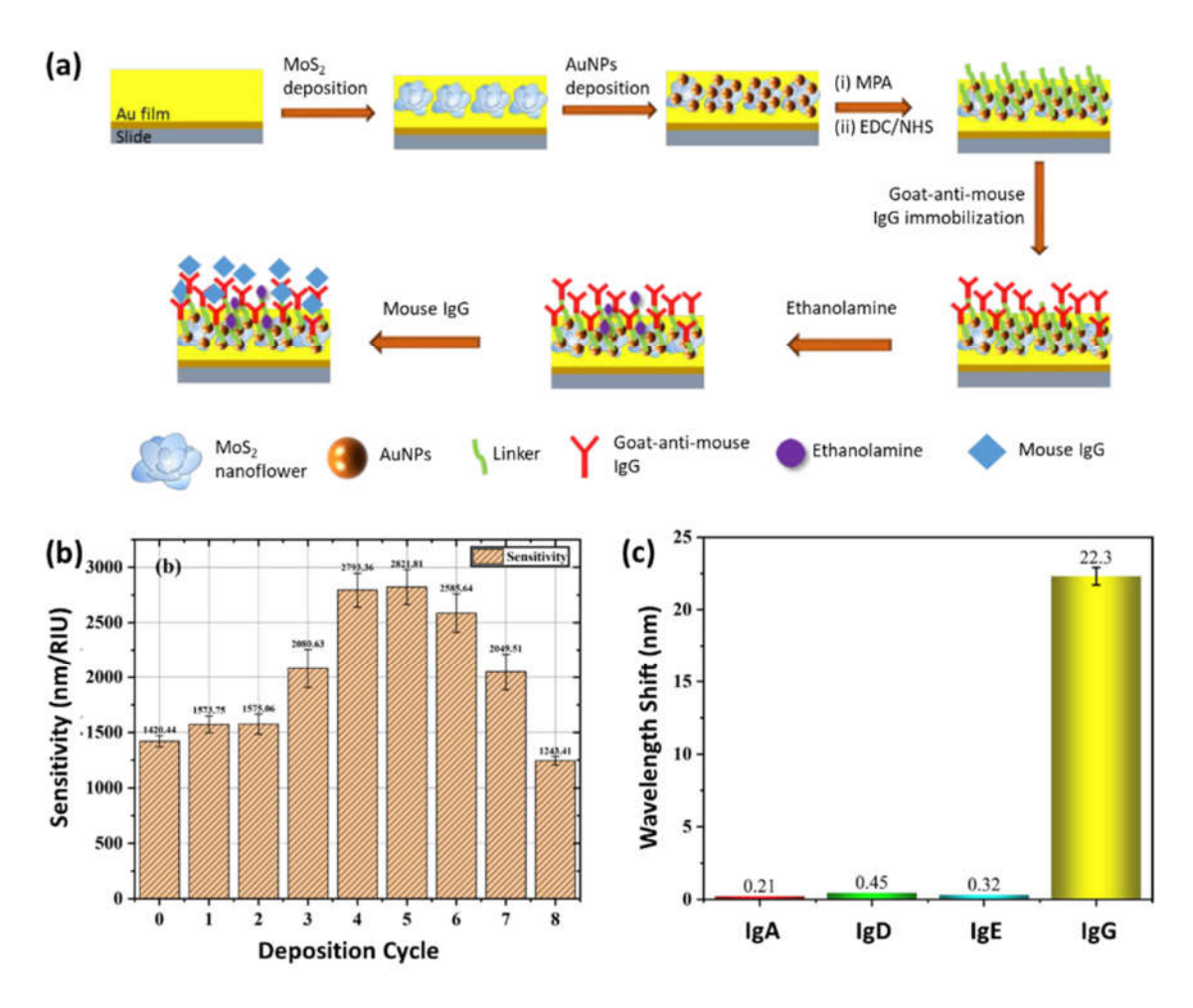


Figure 8 (a) Schematic diagrams of the MoS₂-nanoflowers-based SPR sensor fabrication. Reproduced with permission from ref [26]. Copyright 2020 Royal Chemical Society; (b) Sensitivity of MoSe₂-Au optical fiber SPR sensor with different deposition cycles from 0 to 8. Reproduced with permission from ref [37]. Copyright 2019 IEEE; (c) Resonance wavelength shift of MoS₂-based SPR sensors when detects different kinds of proteins. Reproduced with permission from ref [94]. Copyright 2020 Elsevier.

Table 2. Summary of studies related to TMDCs-based SPR sensors and their performance enhancement.

Hybrid Structure	Methods	Bioreceptors	Analytes	Enhancement Mechanism	Performance	Ref.
Ag/Au/WS ₂ /graphene	Simulation using transfer	-	Bulk	 The sensitivity enhances ~20.5% 	S = 182.5 deg/RIU	[171]
	matrix methods		refractive	compared to bare Ag/Au		
			index	 WS₂ provided low minimum 		
				reflectivity, which indicates good		
-			=	promotion of light absorption		
$Ag/graphene/WS_2$	Simulation using transfer	1	Bulk	 WS₂ helps to improve the sensor 	S = 336 deg/RIU	[172]
	matrix methods		refractive	performance due to the high loss of		
			index	energy led by the silver layer		
Au/MoS ₂ /graphene	Simulation using transfer Probe DNA	Probe DNA	DNA	 The MoS₂ enhances the sensitivity of 	S = 89.29 deg/RIU	[141]
	matrix methods		mismatch	graphene-based sensors by 10%		
				 This enhanced sensitivity occurs due 		
				to the high fluorescence quenching		
Ag/MoSe ₂ /graphene	Simulation using transfer	1	Bulk	The sensitivity is 2.42 times higher	S = 215.5 deg/RIU	[173]
	matrix methods		refractive	than sensors with bare Ag and 2.35	i	
			index	times higher than graphene-based		
				sensors		
Au/MoS ₂ /silicone ¹	Simulation using transfer	-	Bulk	 The silicon nanosheet, together with 	$^{1}\text{S} = 131.70 \text{ deg/RIU}$	[176]
Au/MoSe ₂ /silicone ²	matrix methods		refractive	TMDCs, could accomplish the SPR	$^{2}S = 131.68 \text{ deg/RIU}$	
Au/WS ₂ /silicone ³			index	effect	3 S = 155.68 deg/RIU	
Au/WSe ₂ /silicone ⁴					$^{4}S = 141.40 \text{ deg/RIU}$	
Au/MoS ₂ /Au/MXene ¹	Simulation		Bulk	• The sensitivity of WS ₂ -modified	$^{1}S = 174 \text{ deg/RIU}$	[177]
Au/MoSe ₂ /Au/MXene ²			refractive	sensors increased by 41.43%	2 S = 176 deg/RIU	
Au/WS ₂ /Au/MXene ³			index	compared to conventional SPR	³ S = 198 deg/RIU ⁴ S – 192 deg/RIII	
ZnO/Au/BlueP-MoS ₂	Simulation using transfer		Bulk	• The BlueP-MoS ₂ heterostructure	S = 235 deg/RIU	[106]
	matrix method, field		refractive	generates a more significant number		
	tracing method, and		index	of SPs the on sensors interface		
	resultant wave method			increases the light interaction		

Table 2 Continued. Summary of studies related to TMDCs-based SPR sensors and their performance enhancement.

Hybrid Structure	Methods	Bioreceptors	Analytes	Enhancement Mechanism	Performance	Ref.
Ag/MoS ₂ monolayer	Chemical vapor deposition	Anti-lgG	lgG	 The sensitivity increases by 25% from the bare Ag MoS₂ to avoid oxidation of Ag and degradation of SPR signal 	S = 0.25 degrees from PBS to lgG	[189]
Au/MoS ₂	Drop casting methods	1	Bulk refractive index	• The sensitivity is enhanced by 30.67% compared to bare Au sensors	S = 2793.5 nm/RIU	[92]
Au/MoS ₂ nanoflower ¹ Au/MoS ₂ nanoflower/AuNPs ²	Hydrothermal and drop- casting methods	Anti-mouse IgG	Mouse IgG	The AuNPs provide an ideal platform for immobilization of bioreceptors	¹ S = 0.016 nm/(µg/mL) ² S = 0.0472 nm/(µg/mL)	[26]
Fiber/Au/MoS ₂ ¹ Fiber/MoS₂/Au²	Electrostatic self- assembly	Anti-human IgG	Human IgG	 The high optical absorption of MoS₂ provides higher light energy transmitted from fiber to gold films The sensitivity was increased by 27 – 59% 	¹ S = 4946.8 nm/RIU ² S = 6184.4 nm/RIU	[91]
Fiber/Au/MoS ₂	Liquid exfoliation and dip coating technique	E. coli monoclonal antibodies	E. coli	 The large surface of MoS₂ increases the binding densities of monoclonal antibodies The higher refractive index of the MoS₂ nanosheet allows a more evanescent field in the bioreceptor region 	LOD = 94 CFU/mL	[193]
Fiber/Ag/Au/MoS ₂	Dip coating technique	ı	Bulk refractive index	• The sensitivity was increased by 23% compared to bare bimetallic sensors	S = 3061 nm/RIU	[63]
Fiber/Au/MoSe ₂	Dip coating technique	Rabbit-IgG	Goat anti- rabbit IgG	 Sensitivity 2x higher than fiber Au coated MoSe₂ enhances the loading surface area 	S = 2821.81 nm/RIU LOD = 0.33 µg/mL	[37]

MXene-based SPR Sensor

MXene is known as a new family of 2D materials with remarkable properties that are beneficial for SPR applications, including large surface area and interlayer spacing, adjustable band gap [177], high electrical conductivity [195, 196], and hydrophilic surface [197]. During the synthesis process, abundant surface functionalities naturally owned by the MXene became suitable binding sites for biomolecular targets [108, 116]. Supported by the tremendous optical absorption and bulk plasmonic behaviors on single or multiple layers of MXene, the sensitivity of the MXene-based SPR sensor could be enhanced [131, 135]. Generally, MXene consists of transition metal and carbides, nitrides, or carbonitrides, which provides various possible compounds to be explored. However, the transition metal carbides, especially titanium carbides (Ti₃C₂T_x), are the most studied MXene for improving SPR sensor performance. The titanium has a high absorption affinity and is rich in the hydroxyl group, which can optimize the immobilization of target detection on the sensor surface [198, 199]. The carbides were used due to better stability and the simpler synthesis process than nitrides [200, 201]. A study among MXene-based SPR sensors is commonly limited to simulation or numerical studies, while experimental research is still rare.

The TMM was used to calculate the elements for simulating the SPR phenomenon on metal thin film/Ti₃C₂T_x systems. In the Wu et al. (2018) study, the number of MXene layers and thin film material was varied to obtain the optimum sensitivity enhancement compared to conventional SPR sensors [202]. SPR achieved the highest sensitivity of 160 deg/RIU with four layers of MXene, where the sensitivity was increased by 16.8%. However, adding layers did not increase the sensitivity further (see Figure 9(a)). Since Au is the most chemically stable metal, other metals such as Ag, Al, and Cu are rarely used in SPR sensors. However, the MXene can also function as a protective layer, thus opening up opportunities for using these metals thin film. Finally, the study revealed the sensitivities for Au-, Ag-, Al-, and Cu-based sensors are 160 deg/RIU, 149 deg/RIU, 139 deg/RIU, and 147 deg/RIU, respectively [200]. In wavelength modulation, the experimental study of the sensor with Au/Ti₂C shows a sensitivity of 3579.6 nm/RIU [203]. The Ti₂C was prepared by fluoride etching of Ti₂CAl and deposited on the Au surface by spin-coating. In line with the simulation results by Wu et al. (2019) [202], the maximum number of layers shown in this study is four. Since the titanium shows high affinity to heavy metal ions [198], the sensor was measured to detect Pb²⁺, Cr²⁺, and Hg²⁺, resulting in a sensitivity of 3.788 nm(μ g/L)⁻¹, 5.308 nm(μ g/L)⁻¹, and 3.223 nm(μ g/L)⁻¹, respectively [203].

Various studies also combine MXene with other 2D materials in their hybrid structure to achieve sensor enhancement. The most popular 2D material, graphene, was inserted between the Au thin film and Ti₃C₂T_x layer in the fiber SPR sensor, this structure was studied using TMM [204]. Graphene has a strong coupling of charge carriers, which can increase the electric field in MXene-based SPR sensors. Sensors with ten layers of graphene and three layers of Ti₃C₂T_x provide an extraordinary sensitivity of 5150 nm/RIU, this sensitivity is increased by 43.9% compared to single 2D materials MXene sensors. The sensor sensitivity is still 25.7% and 17.3% higher than MXene-based SPR sensors, even when Ag and Al thin films were used as a substrate [204]. This structure can give cost-efficient fabrication, considering that Ag and Al thin films are cheaper than Au. In the previous section, the hybrid structure that used MXene and TMDCs was investigated, and it was concluded the Au/WS₂/Au/Ti₃C₂T_x was a structure with the highest sensitivity. Srivastava et al. (2020) studied the four different hybrid structures, including conventional sensor (structure 1), BP-modified sensor (structure 2), MXene and BPmodified sensor (structure 3), and MXene, WS2, BP-modified sensor (structure 4) [203]. The sensitivity for each structure is 164.4 deg/RIU, 178.76 deg/RIU, 184.49 deg/RIU, and 190.22 deg/RIU, respectively. The variation of sensitivity as a function of refractive index is shown in Figure 9(b) [205]. Structure 4 of Au/Ti₃C₂T_x/WS₂/BP showed the highest sensitivity enhancement of 15.59% compared to the conventional sensor, as discussed in the previous section, the WS₂ is indeed superior among other TMDC materials [171, 176, 177].

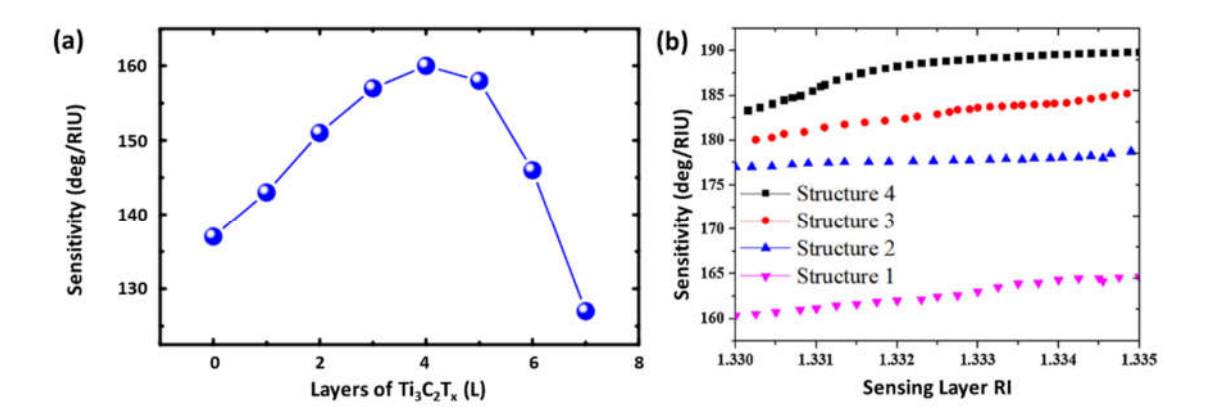


Figure 9 (a) Variation of sensitivity concerning the different number of $Ti_3C_2T_x$ MXene layers . Reproduced with permission from ref [202]. Copyright 2018 Elsevier; (b) Reproduced with permission from ref [205]. Copyright 2018 Elsevier.

Kumar et al. (2021) used the different structures of MXene and BP-modified SPR sensors, significantly enhancing sensitivity. The sensor consists of Cu/Ni as a thin metal film and BP/Ti $_3$ C $_2$ T $_x$ as an immobilization matrix and sensing surface. Using TMM calculation, the sensitivity obtained is 304.47 deg/RIU, which is 85% higher than conventional bare Au sensors. The result indicates the vital role of bimetal, MXene, and BP [206]. In a different study, bimetallic Ag/Au was applied on an MXene-based SPR sensor, resulting in high sensitivity to bulk RI of glucose measurement of 224.18 deg/RIU. The adhesion material applied under the metal thin film was also found to affect the sensor performance, where the comparison showed that metal oxide (MgO) shifted the curve further than polymer (PMMA) [207]. Kumar et al. (2021) applied silicon (Si) between the Ag thin film and MXene layers. The study compares the proposed design with bare Ag and Ag/MXene configurations. The proposed design provided a higher sensitivity of 231 deg/RIU, meanwhile, the bare Ag and Ag/MXene configurations have a sensitivity of 116 deg/RIU and 120.5 deg/RIU, respectively. In numerous studies, Si application resulted in the sensitivity enhancement of the sensor due to its high refractive index, which increases the transverse magnetic field in the sensing region [208].

Table 3. Summary of studies on MXene-based SPR sensor and its performance enhancement.

וואמוות אוותכוחוב	Methods	Bioreceptors	Analytes	Enhancement Mechanism	Performance	Ref.
Ag/MoS ₂ monolayer	Chemical vapor deposition		lgG	 The sensitivity increases by 25% from the bare Ag MoS₂ to avoid oxidation of Ag and degradation of SPR signal 	S = 0.25 degrees from PBS to IgG	[189]
Au/MoS ₂	Drop casting methods	1	Bulk refractive index	• The sensitivity is enhanced by 30.67% compared to bare Au sensors	S = 2793.5 nm/RIU	[65]
Au/MoS ₂ nanoflower ¹ Au/MoS ₂ nanoflower/AuNPs ²	Hydrothermal and drop- casting methods	Anti-mouse IgG	Mouse IgG	The AuNPs provide an ideal platform for immobilization of bioreceptors	¹ S = 0.016 nm/(μg/mL) ² S = 0.0472 nm/(μg/mL)	[26]
Fiber/Au/MoS ₂ 1 Fiber/MoS ₂ /Au ²	Electrostatic self-assembly	Anti-human IgG	Human IgG	 The high optical absorption of MoS₂ provides higher light energy transmitted from fiber to gold films The sensitivity was increased by 27 – 59% 	¹ 5 = 4946.8 nm/RIU ² 5 = 6184.4 nm/RIU	[91]
Fiber/Au/MoS ₂	Liquid exfoliation and dip coating technique	E. coli monoclonal antibodies	E. coli	 The large surface of MoS₂ increases the binding densities of monoclonal antibodies The higher refractive index of the MoS₂ nanosheet allows a more evanescent field in the bioreceptor region 	LOD = 94 CFU/mL	[193]
Fiber/Ag/Au/MoS ₂	Dip coating technique	1	Bulk refractive index	The sensitivity was increased by 23% compared to bare bimetallic sensors	S = 3061 nm/RIU	[63]
Fiber/Au/MoSe ₂	Dip coating technique	Rabbit-IgG	Goat anti- rabbit IgG	 Sensitivity 2x higher than fiber Au coated MoSe₂ enhances the loading surface area 	S = 2821.81 nm/RIU LOD = 0.33 µg/mL	[37]

Table 3 Continued. Summary of studies on MXene-based SPR sensor and its performance enhancement.

Hybrid Structure	Methods		Bioreceptors	Analytes	F	Enhancement Mechanism	Mechanis	E		Performance	Ref.
Cu/Ti ₃ C ₂ T _x ¹	Simulation	using	_	Bulk	•	The prop	s pasod	tructure	was	The proposed structure was ¹ S = 111 deg/RIU	[506]
$Cu/Ni/Ti_3C_2T_x^2$	transfer	matrix		refractive		enhanced	sensitivity	by 1759	6 and	enhanced sensitivity by 175% and ${}^{2}S = 261 \text{ deg/RIU}$	
$Cu/Ni/BP/Ti_3C_2T_x^3$	method			index		25% to Cu/	Ti ₃ C ₂ T _x and	d Cu/Ni/T	i ₃ C ₂ T _x ,	25% to $Cu/Ti_3C_2T_x$ and $Cu/Ni/Ti_3C_2T_x$, $^3S = 304.47 \text{ deg/RIU}$	Ω
						respectively	^				
					•	Compared to the bare Au sensor,	to the b	are Au s	ensor,		
						the sensitivity increased by 85%	ity increa	sed by 85	%		
$MgO/Ag/Au/Ti_3C_2T_x$	Simulation	using	ı	Sugar	•	MXene functioned as	function	ed as		a S = 224.18 deg/RIU [207]	J [207]
	transfer	matrix				biorecognition element that	tion eler	nent th	at is		
	method					suitable for sugar detection	r sugar det	tection			
Ag/Si/Ti ₃ C ₂ T _x	Simulation using the	sing the	-	Bulk	•	The bir	oding c	apability	of	The binding capability of S = 231 deg/RIU	[508]
	transfer	matrix		refractive		biomolecules on MXene surface	les on N	AXene s	urface		
	method			index		owing to its larger surface area,	its larger	surface	area,		
						chemical stability, and excellent	stability,	and exc	ellent		
						absorption property	property				

Other 2D Material in SPR Sensor

Since graphene was successfully fabricated by mechanical exfoliation from graphite in 2004 [56], various 2D materials have been developed and applied in SPR sensors in the last decade. SPR sensors, which used graphene, TMDCs, and MXene, have been detailed and discussed in the previous section. In this section, the study relating to other 2D materials, namely black phosphorus (BP), perovskite, and boron nitride (BN), will be reviewed simultaneously because of the lack of study that focuses on each material in SPR application.

BP is known as a 2D material with remarkable electrical and optical properties and a high surface-to-volume ratio because of its puckered configuration [209]. Thus, the BP-based sensors are reported to perform the detection 40 times faster and 20 times higher molar response than other 2D materials [210]. The BP-modified SPR sensor has been shown to increase the sensitivity by at least 51% in structures with single 2D materials of BP [211]. The performance of BP-based sensors gets higher when combined with other 2D materials such as graphene, TMDCs, and MXene, which enhance 87 – 140% [159, 211]. The detailed performance for each sensor based on hybrid 2D materials with BP has been described in the previous section and shown in Table 4. As shown in Figure 10(a), the changes in the number of layers of BP affect the SPR response curve, where increasing the number of layers makes the angle wider, with the reflectivity tending to be constant. The low extinction coefficient of BP causes the condition; the wave vector of surface plasmons shifts to satisfy the resonance condition at the resonance angle [148]. The shifts and broadening of the SPR curve are related to sensor performance, where the more layers, the greater the sensitivity and FOM (see Figure 10(b)). However, the increment will occur until a certain thickness and will saturate due to more layer addition, as observed in other 2D materials [158]. As found in other 2D materials-based SPR, the addition of Si between thin metal films and BP provides the most significant enhancement in sensitivity due to an increase in the intensity of the surface field due to the high refractive index [212].

Perovskite is a new type of plasmonic material that promises excellent optical and electrical properties with an inexpensive process needed in the fabrication [213]. 2D perovskite arising the quantum confinement and excitonic effect, which is advantageous for the plasmonic application, including SPR sensors [214-217]. The perovskite-based SPR sensor has been reported by Hakami et al. (2021), which used two types of methylammonium lead halide perovskites, namely MaPbl3 and MaPbBr3 in the sensor systems Ag/TiO2/perovskite [213]. The TiO₂ provides field confinement and enhancement at the metal-dielectric interface due to its high refractive index [218]. The TMM simulation calculates the SPR sensor performance in perovskite- and nonperovskite-based sensors. The best performance is provided by the MaPbI3 followed by MaPbBr3 and nonperovskite sensors as indicated by its reflectivity and sensitivity of 143.80 deg/RIU, 140.60 deg/RIU, and 136.60 deg/RIU, respectively. The presence of perovskite materials increased the sensitivity by 2 - 5% compared to the bare sensors in measuring bulk refractive index. Contrary to structure Ag/TiO2/perovskite/graphene, the best sensitivity performance is obtained by MaPbBr3 at 255.80 deg/RIU and MaPbI3 at 250.20 deg/RIU. Meanwhile, for the detection of glucose, the sensors also produce a fair sensitivity of 0.0212 deg/gL⁻¹ for both perovskite materials [213]. In other studies, the WS₂ TMDCs are used to feature with MaPbl₃ in bimetallic SPR sensors. The high sensitivity of 195 deg/RIU was reached by sensors with 1.7 nm MaPbl₃, which is much higher than the bare bimetallic sensors sensitivity of 145 deg/RIU [219]. Surprisingly, the significant enhancement to 370 deg/RIU was reached when more and more 2D materials were applied, including TMDCs, perovskite, and BP in structure Ag/WS₂/BaTiO₃/BP as shown in Figure 10(c) [220].

Another 2D material that has not been studied much is boron nitride or hexagonal boron nitride (h-BN). 2D h-BN is known for its large surface area, wide bandgap, and high conductivity, making it suitable for sensor applications, wrapping materials in solar cells, and catalysis [221, 222]. The hBN nanosheets can be obtained from the ultrasonication-assisted exfoliation of bulk boron nitride [222]. The SPR sensor of Au/Ag@AuNPs-hBN with morphology-imprinted (MIP) was used to measure the presence of ETO anticancer drugs and reach the LOD of 4.25×10^{-13} mol/L which is around five times lower than other methods [223]. The sensorgrams indicated the selectivity of sensors. As shown in Figure 10(d), the highest absorption capacity (Δ R) is obtained when the sensor detects the ETO, it was 48, 24, 12, 6, and 4 times more selective compared to citric acid, uric acid, ascorbic acid, sucrose, and glucose [223]. Unfortunately, due to limited reports regarding hBN-based SPR sensors, the performance of sensors with structural and material modifications cannot be discussed in this review.

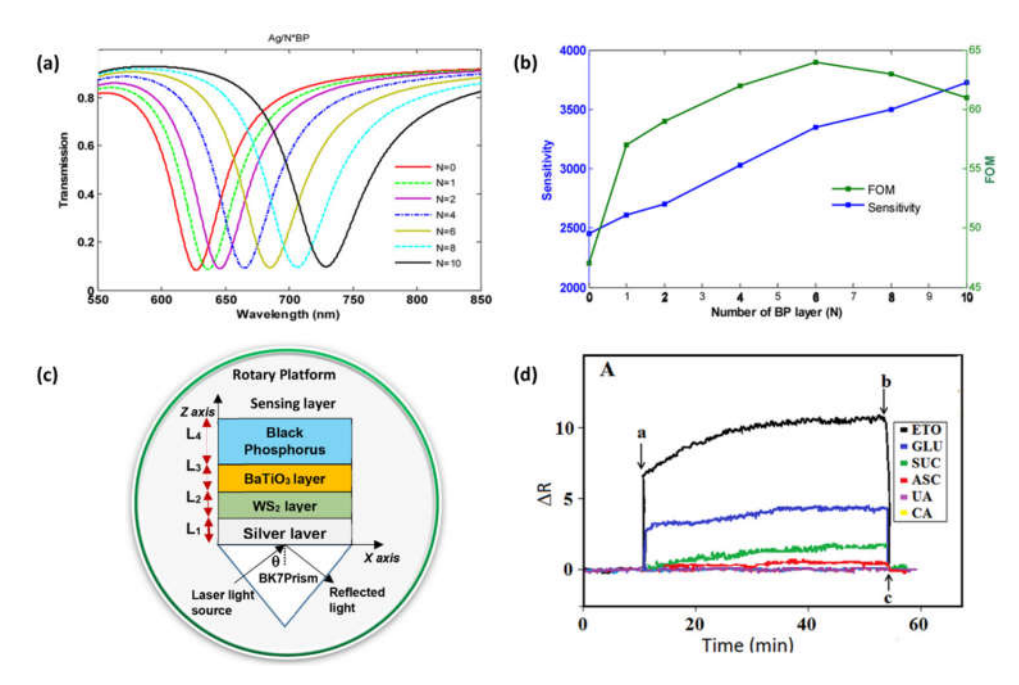


Figure 10 (a) SPR response curve and (b) sensitivity and figure of merit (FOM) for different layers of black phosphorene (BP) over the Ag film. Reproduced with permission from ref [158]. Copyright 2019 Elsevier; (c) Schematic diagram of proposed WS₂/BaTiO₃/black phosphorus-based SPR biosensor. Reproduced with permission from ref [220]. Copyright 2020 Wiley; (d) Sensorgrams relating to 1.0 ng/mL ETO, GLU, SUC, ASC, UA and CA on NIP/Ag@AuNPs-hBN/SPR with binding activity a) adsorption; b) desorption; c) regeneration. Reproduced with permission from ref [223]. Copyright 2019 Elsevier.

Conclusions and Outlook

The outstanding capabilities of elemental 2D materials enable future breakthroughs toward high-performance sensing devices. Many elemental 2D materials denote advantageous features for sensor systems, especially SPR biosensors, such as high electron and hole mobility, high optical absorption, high surface-to-volume ratio, and suitable binding sites. Furthermore, 2D materials in SPR sensors possess some merits and different characteristics for each member of the 2D materials family, depending on the composition. Graphene is well-known as an inert and zero-gap materials with broad-band and relatively high light absorption. Its derivatives, graphene oxide, provide rich functional groups suitable for immobilizing bioreceptors or ligands. Likewise, in MXene functional groups such as -H, -F, -OH, or -O can increase the ability to bind the bioreceptors and target detection. TMDCs do not own these chemically active sites. However, TMDCs excel in their tunable bandgap characteristics and stronger absorption in the NIR-to-visible range. The bandgap tuning can also be performed in MXene by adjusting several factors such as strain and external field, this feature supports optimization of material performance for specific applications.

However, some shortcomings still need to be investigated in developing 2D materials-based SPR sensors. Due to the following limitations, 2D materials-based SPR detection has been limited to laboratory use and lags considerably behind other sectors. Firstly, even in stable and controlled conditions, 2D material films have a short lifetime because of the aging, oxidation, and peeling processes. This characteristic has limited the reusability of 2D materials-based SPR sensors. Secondly, various studies have shown that the optimum thickness of 2D materials is <10 layers, but the fabrication of a few layers of 2D materials can only be done through expensive techniques such as CVD, ALD, and PLD. The agglomeration behavior of 2D materials makes fabricating through a solution-based deposition challenging. Lastly, the lack of active sites in several 2D materials should be overcome for various actions and selectivity.

Most 2D materials in SPR investigations are limited to simulations and numerical studies. Moreover, the variation of detection targets analyzed commonly only measures the sensitivity of the sensor to changes in bulk refractive index. Thus, knowledge regarding the interaction and immobilization of bioreceptors and targets on the surface of 2D materials is still limited. The numerous studies only provide a sensitivity of sensors, whereas the limit-of-detection is also a vital figure of merit to represent sensor performance. The primary goals of future study in 2D materials-based SPR sensors should be directed towards realizing a device fabrication process with low cost and more scalable techniques. The fabrication process must also ensure long-term environmental stability and prevent material deterioration, which must be considered according to the application. However, the various significant challenges that must be faced are worth the exceptional 2D material properties, guaranteeing a massive contribution to developing sensor technology and other technologies such as nanoelectronics, photonics, and energy systems.

References

- [1] Mariani, S. & Minunni, M., *Surface Plasmon Resonance Applications in Clinical Analysis,* Analytical and Bioanalytical Chemistry, **406**, pp. 2303-2323, 2014.
- [2] Liedberg, B., Nylander, C. & Lunström, I., Surface Plasmon Resonance for Gas Detection and Biosensing, Sensors and Actuators, 4, pp. 299-304, 1983.
- [3] Rebe Raz, S., Leontaridou, M., Bremer, M. G., Peters, R. & Weigel, S., *Development of Surface Plasmon Resonance-Based Sensor for Detection of Silver Nanoparticles in Food and the Environment*, Analytical and Bioanalytical Chemistry, **403**, pp. 2843-2850, 2012.
- [4] Shankaran, D.R., Gobi, K.V. & Miura, N., Recent Advancements in Surface Plasmon Resonance Immunosensors for Detection of Small Molecules of Biomedical, Food and Environmental Interest, Sensors and Actuators B: Chemical, 121(1), pp. 158-177, 2007.
- [5] Situ, C., Mooney, M.H., Elliott, C.T. & Buijs, J., Advances in Surface Plasmon Resonance Biosensor Technology Towards High-Throughput, Food-Safety Analysis, TrAC Trends in Analytical Chemistry, **29**(11), pp. 1305-1315, 2010.
- [6] Narsaiah, K., Jha, S.N., Bhardwaj, R., Sharma, R. & Kumar, R., *Optical Biosensors for Food Quality and Safety Assurance—A Review, Journal of Food Science And Technology*, **49**, pp. 383-406, 2012.
- [7] Menon, P.S., Mulyanti, B., Jamil, N.A., Wulandari, C., Nugroho, H.S., Mei, G.S., Abidin, N.F.Z., Hasanah, L., Pawinanto, R.E. & Berhanuddin, D.D., *Refractive Index and Sensing of Glucose Molarities Determined Using Au-Cr K-SPR At 670/785 nm Wavelength*, Sains Malaysiana, **48**(6), pp.1259-1265, 2019.
- [8] Hasanah, L., Nugroho, H.S., Wulandari, C., Mulyanti, B., Berhanuddin, D.D., Haron, M.H., Menon, P.S., Zain, A.R.M., Hamidah, I., Khairurrijal, K. & Mamat, R., Enhanced Sensitivity of Microring Resonator-Based Sensors Using the Finite Difference Time Domain Method to Detect Glucose Levels for Diabetes Monitoring, Applied Sciences, 10(12), 4191, 2020.
- [9] Helmerhorst, E., Chandler, D.J., Nussio, M. & Mamotte, C.D., Real-Time and Label-Free Bio-Sensing of Molecular Interactions by Surface Plasmon Resonance: A Laboratory Medicine Perspective, The Clinical Biochemist Reviews, 33(4), pp. 161-173, 2012.
- [10] Brennan, D., Justice, J., Corbett, B., McCarthy, T. & Galvin, P., *Emerging Optofluidic Technologies for Point-of-Care Genetic Analysis Systems: A Review,* Analytical and Bioanalytical Chemistry, **395**, pp. 621-636, 2009.
- [11] Mishra, S.K., Zou, B. & Chiang, K.S., Surface-Plasmon-Resonance Refractive-Index Sensor with Cu-Coated Polymer Waveguide, IEEE Photonics Technology Letters, 28(17), pp. 1835-1838, 2016.
- [12] Shukla, S., Sharma, N.K. & Sajal, V., Sensitivity Enhancement of A Surface Plasmon Resonance Based Fiber Optic Sensor Using Zno Thin Film: A Theoretical Study, Sensors and Actuators B: Chemical, 206, pp. 463-470, 2015.
- [13] Homola, J., Yee, S.S. & Gauglitz, G., *Surface Plasmon Resonance Sensors*, Sensors and Actuators B: Chemical, **54**(1-2), pp. 3-15, 1999.
- [14] Miyazaki, C.M., Shimizu, F.M. & Ferreira, M., Surface Plasmon Resonance (SPR) for Sensors and Biosensors, in Nanocharacterization Techniques, pp. 183-200, William Andrew Publishing, 2017.
- [15] Mauriz, E., García-Fernández, M.C., & Lechuga, L.M., *Towards the Design of Universal Immunosurfaces For SPR-Based Assays: A Review,* TrAC Trends in Analytical Chemistry, **79**, pp. 191-198, 2016.

[16] Poma, A., Turner, A.P. & Piletsky, S.A., *Advances in the Manufacture of MIP Nanoparticles,* Trends in Biotechnology, **28**(12), pp. 629-637, 2010.

- [17] Šípová, H. & Homola, J., *Surface Plasmon Resonance Sensing of Nucleic Acids: A Review,* Analytica Chimica Acta, **773**, pp. 9-23, 2013.
- [18] Zhou, J., Battig, M.R. & Wang, Y., *Aptamer-Based Molecular Recognition for Biosensor Development,* Analytical and Bioanalytical Chemistry, **398**, pp. 2471-2480, 2010.
- [19] Hashim, H.S., Fen, Y.W., Omar, N.A.S., Abdullah, J., Daniyal, W.M.E.M.M. & Saleviter, S., *Detection of Phenol by Incorporation of Gold Modified-Enzyme Based Graphene Oxide Thin Film with Surface Plasmon Resonance Technique*, Optics Express, **28**(7), pp. 9738-9752, 2020.
- [20] D'Agata, R. & Spoto, G., Artificial DNA and Surface Plasmon Resonance, Artificial DNA: PNA & XNA, 3(2), pp. 45-52, 2012.
- [21] Xiao, S.J., Brunner, S. & Wieland, M., Reactions of Surface Amines with Heterobifunctional Cross-Linkers Bearing Both Succinimidyl Ester and Maleimide for Grafting Biomolecules, The Journal of Physical Chemistry B, **108**(42), pp. 16508-16517, 2004.
- [22] Gunda, N.S.K., Singh, M., Norman, L., Kaur, K. & Mitra, S.K., Optimization and Characterization of Biomolecule Immobilization on Silicon Substrates Using (3-Aminopropyl) Triethoxysilane (APTES) and Glutaraldehyde Linker, Applied Surface Science, 305, pp. 522-530, 2014.
- [23] Kaushik, S., Tiwari, U.K., Deep, A. & Sinha, R.K., *Two-Dimensional Transition Metal Dichalcogenides Assisted Biofunctionalized Optical Fiber SPR Biosensor for Efficient and Rapid Detection of Bovine Serum Albumin*, Scientific Reports, **9**(1), 6987, 2019.
- [24] Mei, G.S., Menon, P.S. & Hegde, G., ZnO for Performance Enhancement of Surface Plasmon Resonance Biosensor: A Review, Materials Research Express, 7(1), 012003, 2020.
- [25] Szunerits, S., Maalouli, N., Wijaya, E., Vilcot, J.P. & Boukherroub, R., Recent Advances in the Development of Graphene-Based Surface Plasmon Resonance (SPR) Interfaces, Analytical and Bioanalytical Chemistry, 405, pp. 1435-1443, 2013.
- [26] Zhao, P., Chen, Y., Chen, Y., Hu, S., Chen, H., Xiao, W., Liu, G., Tang, Y., Shi, J., He, Z., Luo, Y. & Chen, Z., A MoS 2 Nanoflower and Gold Nanoparticle-Modified Surface Plasmon Resonance Biosensor for a Sensitivity-Improved Immunoassay, Journal of Materials Chemistry C, 8(20), pp. 6861-6868, 2020.
- [27] Oh, S., Moon, J., Kang, T., Hong, S. & Yi, J., Enhancement of Surface Plasmon Resonance (SPR) Signals Using Organic Functionalized Mesoporous Silica on a Gold Film, Sensors and Actuators B: Chemical, 114(2), pp. 1096-1099, 2006.
- [28] Xiao, M., Wei, S., Chen, J., Tian, J., Brooks III, C.L., Marsh, E.N.G. & Chen, Z., *Molecular Mechanisms of Interactions between Monolayered Transition Metal Dichalcogenides and Biological Molecules*, Journal of the American Chemical Society, **141**(25), pp. 9980-9988, 2019.
- [29] Peng, C. & Zhang, X., Chemical Functionalization of Graphene Nanoplatelets with Hydroxyl, Amino, and Carboxylic Terminal Groups, Chemistry, **3**(3), pp. 873-888, 2021.
- [30] Wang, Q.H., Kalantar-Zadeh, K., Kis, A., Coleman, J.N. & Strano, M.S., *Electronics and Optoelectronics of Two-Dimensional Transition Metal Dichalcogenides*, Nature Nanotechnology, **7**(11), pp. 699-712, 2012.
- [31] Geim, A.K., *Graphene: Status and Prospects,* Science, **324**(5934), pp. 1530-1534, 2009.
- [32] Xu, X., Yao, W., Xiao, D. & Heinz, T.F., Spin and Pseudospins in Layered Transition Metal Dichalcogenides, Nature Physics, 10(5), pp. 343-350, 2014.
- [33] Xiao, D., Liu, G.B., Feng, W., Xu, X. & Yao, W., Coupled Spin and Valley Physics in Monolayers of MoS2 and other Group-VI Dichalcogenides, Physical Review Letters, **108**(19), 196802, 2012.
- [34] Mak, K.F., Lee, C., Hone, J., Shan, J. & Heinz, T.F., Atomically Thin MoS2: A New Direct-Gap Semiconductor, Physical Review Letters, 105(13), 136805, 2010.
- [35] Bonaccorso, F., Sun, Z., Hasan, T. & Ferrari, A.C., *Graphene Photonics and Optoelectronics*, Nature Photonics, **4**(9), pp. 611-622, 2010.
- [36] Xia, F., Wang, H., Xiao, D., Dubey, M. & Ramasubramaniam, A., *Two-Dimensional Material Nanophotonics*, Nature Photonics, **8**(12), pp. 899-907, 2014.
- [37] Liu, K., Zhang, J., Jiang, J., Xu, T., Wang, S., Chang, P., Zhang, Z., Ma, Z. & Liu, T., MoSe2-Au based Sensitivity Enhanced Optical Fiber Surface Plasmon Resonance Biosensor for Detection of Goat-Anti-Rabbit IgG, IEEE Access, 8, pp. 660-668, 2019.
- [38] Kumar, R., Kushwaha, A.S., Srivastava, M., Mishra, H. & Srivastava, S.K., Enhancement in Sensitivity of Graphene-Based Zinc Oxide Assisted Bimetallic Surface Plasmon Resonance (SPR) Biosensor, Applied Physics A, 124, pp. 1-10, 2018.

- [39] Kretschmann, E. & Raether, H., Radiative Decay of Non Radiative Surface Plasmons Excited by Light, Zeitschrift für Naturforschung A, 23(12), pp. 2135-2136, 1968.
- [40] Homola, J., Surface Plasmon Resonance Sensors for Detection of Chemical and Biological Species, Chemical Reviews, **108**(2), pp. 462-493, 2008.
- [41] Hinman, S.S., McKeating, K.S. & Cheng, Q., Surface Plasmon Resonance: Material and Interface Design for Universal Accessibility, Analytical Chemistry, **90**(1), pp. 19-39, 2018.
- [42] Zhu, J. & Li, N., Novel High Sensitivity SPR Sensor Based on Surface Plasmon Resonance Technology and IMI Waveguide Structure, Results in Physics, 17, 103049, 2020.
- [43] Du, W., Miller, L. & Zhao, F., *Numerical Study of Graphene/Au/Sic Waveguide-Based Surface Plasmon Resonance Sensor*, Biosensors, **11**(11), 455, 2021.
- [44] Dai, Y., Xu, H., Wang, H., Lu, Y. & Wang, P., Experimental Demonstration of High Sensitivity for Silver Rectangular Grating-Coupled Surface Plasmon Resonance (SPR) Sensing, Optics Communications, **416**, pp. 66-70, 2018.
- [45] Zeng, L., Chen, M., Yan, W., Li, Z. & Yang, F., Si-Grating-Assisted SPR Sensor with High Figure of Merit Based on Fabry–Pérot Cavity, Optics Communications, **457**, 124641, 2020.
- [46] Pandey, P.S., Raghuwanshi, S.K. & Kumar, S., Recent Advances in Two-Dimensional Materials-Based Kretschmann Configuration for SPR Sensors: A Review, IEEE Sensors Journal, 22(2), pp. 1069-1080, 2021.
- [47] Taya, S.A., *P-Polarized Surface Waves in a Slab Waveguide with Left-Handed Material for Sensing Applications*, Journal of Magnetism and Magnetic Materials, **377**, pp. 281-285, 2015.
- [48] Qu, J.H., Dillen, A., Saeys, W., Lammertyn, J. & Spasic, D., Advancements in SPR Biosensing Technology: An Overview of Recent Trends in Smart Layers Design, Multiplexing Concepts, Continuous Monitoring and In Vivo Sensing, Analytica Chimica Acta, 1104, pp. 10-27, 2020.
- [49] Abadla, M.M., & Taya, S.A., Excitation of TE Surface Polaritons on Metal–NIM Interfaces, Optik, 125(3), pp. 1401-1405, 2014.
- [50] Gupta, B.D., Shrivastav, A.M. & Usha, S.P., Surface Plasmon Resonance-Based Fiber Optic Sensors Utilizing Molecular Imprinting, Sensors, 16(9), 1381, 2016.
- [51] Malachovska, V., Ribaut, C., Voisin, V., Surin, M., Leclere, P., Wattiez, R. & Caucheteur, C., Fiber-Optic SPR Immunosensors Tailored to Target Epithelial Cells Through Membrane Receptors, Analytical Chemistry, 87(12), pp. 5957-5965, 2015.
- [52] Zhao, Y., Hu, X. G., Hu, S. & Peng, Y., *Applications of Fiber-Optic Biochemical Sensor in Microfluidic Chips: A Review,* Biosensors and Bioelectronics, **166**, 112447, 2020.
- [53] Moradi, V., Akbari, M. & Wild, P., A Fluorescence-Based Ph Sensor with Microfluidic Mixing and Fiber Optic Detection for Wide Range Ph Measurements, Sensors and Actuators A: Physical, **297**, pp. 111507, 2019.
- [54] Arghir, I., Delport, F., Spasic, D. & Lammertyn, J., Smart Design of Fiber Optic Surfaces for Improved Plasmonic Biosensing, New Biotechnology, **32**(5), pp. 473-484, 2015.
- [55] Caucheteur, C., Guo, T. & Albert, J., Review of Plasmonic Fiber Optic Biochemical Sensors: Improving the Limit of Detection, Analytical and Bioanalytical Chemistry, **407**, pp. 3883-3897, 2015.
- [56] Novoselov, K.S., Geim, A.K., Morozov, S.V., Jiang, D.E., Zhang, Y., Dubonos, S.V., Grigorieva, I.V. & Firsov, A.A., *Electric Field Effect in Atomically Thin Carbon Films, Science*, **306**(5696), pp. 666-669, 2004.
- [57] Bolotin, K I., Sikes, K.J., Jiang, Z., Klima, M., Fudenberg, G., Hone, J., Kim, P. & Stormer, H.L., *Ultrahigh Electron Mobility in Suspended Graphene*, Solid State Communications, **146**(9-10), pp. 351-355, 2008.
- [58] Balandin, A.A., Ghosh, S., Bao, W., Calizo, I., Teweldebrhan, D., Miao, F. & Lau, C.N., Superior Thermal Conductivity of Single-Layer Graphene, Nano Letters, 8(3), pp. 902-907, 2008.
- [59] Lee, C., Wei, X., Kysar, J.W. & Hone, J., Measurement of the Elastic Properties and Intrinsic Strength of Monolayer Graphene, Science, **321**(5887), pp. 385-388, 2008.
- [60] Nair, R.R., Blake, P., Grigorenko, A.N., Novoselov, K.S., Booth, T.J., Stauber, T., Peres, N.M.R. & Geim, A.K., Fine Structure Constant Defines Visual Transparency of Graphene, Science, 320(5881), pp. 1308-1308, 2008.
- [61] Zeng, M., Xiao, Y., Liu, J., Lu, W. & Fu, L., Controllable Fabrication of Nanostructured Graphene towards *Electronics*, Advanced Electronic Materials, **2**(4), 1500456, 2016.
- [62] Stanford, M.G., Zhang, C., Fowlkes, J.D., Hoffman, A., Ivanov, I.N., Rack, P.D. & Tour, J.M., High-Resolution Laser-Induced Graphene. Flexible Electronics Beyond the Visible Limit, ACS Applied Materials & Interfaces, 12(9), pp. 10902-10907, 2020.
- [63] Polat, E.O., Uzlu, H.B., Balci, O., Kakenov, N., Kovalska, E. & Kocabas, C., *Graphene-Enabled Optoelectronics on Paper*, ACS Photonics, **3**(6), pp.964-971, 2016.

[64] Zhang, Z., Lin, P., Liao, Q., Kang, Z., Si, H. & Zhang, Y., *Graphene-Based Mixed-Dimensional Van Der Waals Heterostructures for Advanced Optoelectronics*, Advanced Materials, **31**(37), 1806411, 2019.

- [65] Bonaccorso, F., Sun, Z., Hasan, T. & Ferrari, A.C., *Graphene Photonics and Optoelectronics*, Nature Photonics, **4**(9), pp. 611-622, 2010.
- [66] Wang, J., Ma, F., & Sun, M., *Graphene, Hexagonal Boron Nitride, and Their Heterostructures: Properties and Applications*, RSC Advances, **7**(27), pp. 16801-16822, 2017.
- [67] Yu, W., Sisi, L., Haiyan, Y. & Jie, L., *Progress in The Functional Modification of Graphene/Graphene Oxide:* A Review, RSC Advances, **10**(26), pp. 15328-15345, 2020.
- [68] Avouris, P., Graphene: Electronic and Photonic Properties and Devices, Nano Letters, 10(11), pp. 4285-4294, 2010
- [69] Wang, X.L., Dou, S.X. & Zhang, C., Zero-gap Materials for Future Spintronics, Electronics and Optics, NPG Asia Materials, 2(1), pp. 31-38, 2010.
- [70] Junaid, M., Khir, M.M., Witjaksono, G., Tansu, N., Saheed, M.S.M., Kumar, P., Ullah, Z., Yar, A. & Usman, F., Boron-Doped Reduced Graphene Oxide with Tunable Bandgap and Enhanced Surface Plasmon Resonance, Molecules, 25(16), 3646, 2020.
- [71] Xu, X., Liu, C., Sun, Z., Cao, T., Zhang, Z., Wang, E., Liu, Z. & Liu, K., *Interfacial Engineering in Graphene Bandgap*, Chemical Society Reviews, **47**(9), pp. 3059-3099, 2018.
- [72] Jiao, L., Zhang, L., Wang, X., Diankov, G. & Dai, H., Narrow Graphene Nanoribbons from Carbon Nanotubes, Nature, 458(7240), pp. 877-880, 2009.
- [73] Cai, J., Ruffieux, P., Jaafar, R., Bieri, M., Braun, T., Blankenburg, S., Muoth, M., Seitsonen, A.P., Saleh, M., Feng, X., Mullen, K. & Fasel, R., *Atomically Precise Bottom-Up Fabrication of Graphene Nanoribbons*, Nature, **466**(7305), pp. 470-473, 2010.
- [74] Park, J., Kim, Y., Park, S.Y., Sung, S.J., Jang, H.W. & Park, C.R., Band Gap Engineering of Graphene Oxide for Ultrasensitive NO2 Gas Sensing, Carbon, 159, pp. 175-184, 2020.
- [75] Du, X., Skachko, I., Barker, A. & Andrei, E.Y, Approaching Ballistic Transport in Suspended Graphene, Nature Nanotechnology, 3(8), pp. 491-495, 2008.
- [76] Kong, L., Enders, A., Rahman, T.S. & Dowben, P.A., *Molecular Adsorption on Graphene*, Journal of Physics: Condensed Matter, **26**(44), 443001, 2014.
- [77] Bhushan, B. (Ed.), *Encyclopedia of Nanotechnology (No. 544.1), Dordrecht*, The Netherlands: Springer, 2012.
- [78] Li, Z., Henriksen, E.A., Jiang, Z., Hao, Z., Martin, M.C., Kim, P., Stormer, H.L. & Basov, D.N., *Dirac Charge Dynamics in Graphene by Infrared Spectroscopy*, Nature Physics, **4**(7), pp. 532-535, 2008.
- [79] Wright, A.R., Cao, J.C. & Zhang, C., Enhanced Optical Conductivity of Bilayer Graphene Nanoribbons in the Terahertz Regime, Physical Review Letters, **103**(20), 207401, 2009.
- [80] Frindt, R.F. & Yoffe, A.D., *Physical Properties of Layer Structures: Optical Properties and Photoconductivity of Thin Crystals of Molybdenum Disulphide,* Proceedings of the Royal Society of London. Series A. Mathematical and Physical Sciences, **273**(1352), pp. 69-83, 1963.
- [81] Joensen, P., Frindt, R.F. & Morrison, S.R., Single-Layer MoS2, Materials Research Bulletin, 21(4), pp. 457-461, 1986.
- [82] Tenne, R., Margulis, L., Genut, M.E. & Hodes, G., *Polyhedral and Cylindrical Structures of Tungsten Disulphide*, Nature, **360**(6403), pp. 444-446, 1992.
- [83] Feldman, Y., Wasserman, E., Srolovitz, D.J. & Tenne, R., *High-Rate, Gas-Phase Growth of MoS2 Nested Inorganic Fullerenes and Nanotubes, Science*, **267**(5195), pp. 222-225, 1995.
- [84] Novoselov, K.S., Jiang, D., Schedin, F., Booth, T.J., Khotkevich, V.V., Morozov, S.V. & Geim, A.K., *Two-dimensional atomic crystals, Proceedings of the National Academy of Sciences*, **102**(30), pp. 10451-10453, 2005.
- [85] Manzeli, S., Ovchinnikov, D., Pasquier, D., Yazyev, O.V. & Kis, A., 2D Transition Metal Dichalcogenides, Nature Reviews Materials, 2(8), pp. 1-15, 2017.
- [86] Cheiwchanchamnangij, T. & Lambrecht, W.R., Quasiparticle Band Structure Calculation of Monolayer, Bilayer, and Bulk MoS2, Physical Review B, 85(20), 205302, 2012.
- [87] Lebegue, S. & Eriksson, O., *Electronic Structure of Two-Dimensional Crystals from Ab Initio Theory,* Physical Review B, **79**(11), 115409, 2009.
- [88] Mak, K.F. & Shan, J., Photonics and Optoelectronics of 2D Semiconductor Transition Metal Dichalcogenides, Nature Photonics, **10**(4), pp. 216-226, 2016.

- [89] Splendiani, A., Sun, L., Zhang, Y., Li, T., Kim, J., Chim, C.Y., Galli, G. & Wang, F., *Emerging Photoluminescence in Monolayer MoS2*, Nano Letters, **10**(4), pp. 1271-1275, 2010.
- [90] Zeng, H., Dai, J., Yao, W., Xiao, D. & Cui, X., Valley Polarization in MoS2 Monolayers by Optical Pumping, Nature Nanotechnology, 7(8), pp. 490-493, 2012.
- [91] Haug, H. & Koch, S.W., *Quantum Theory of the Optical and Electronic Properties of Semiconductors*, World Scientific Publishing Co. Pte. Ltd, 2004.
- [92] Chen, Y., Hu, S., Wang, H., Zhi, Y., Luo, Y., Xiong, X., Dong, J., Jiang, Z., Zhu, W., Qiu, W., Lu, H., Guan, H., Zhong, Y., Yu, J., Zhang, J. & Chen, Z., MoS2 Nanosheets Modified Surface Plasmon Resonance Sensors for Sensitivity Enhancement, Advanced Optical Materials, 7(13), 1900479, 2019.
- [93] Wang, Q., Jiang, X., Niu, L.Y. & Fan, X.C., Enhanced Sensitivity of Bimetallic Optical Fiber SPR Sensor Based on MoS2 Nanosheets, Optics and Lasers in Engineering, 128, 105997, 2020.
- [94] Song, H., Wang, Q. & Zhao, W. M., A Novel SPR Sensor Sensitivity-Enhancing Method for Immunoassay by Inserting MoS2 Nanosheets between Metal Film and Fiber, Optics and Lasers in Engineering, **132**, 106135, 2020.
- [95] Hu, H., Zavabeti, A., Quan, H., Zhu, W., Wei, H., Chen, D. & Ou, J.Z., *Recent Advances in Two-Dimensional Transition Metal Dichalcogenides for Biological Sensing, Biosensors and Bioelectronics*, **142**, 111573, 2019.
- [96] Mak, K.F., He, K., Lee, C., Lee, G.H., Hone, J., Heinz, T.F. & Shan, J., *Tightly Bound Trions in Monolayer MoS2*, Nature Materials, **12**(3), pp. 207-211, 2013.
- [97] Ramasubramaniam, A., Large Excitonic Effects in Monolayers of Molybdenum and Tungsten Dichalcogenides, Physical Review B, **86**(11), 115409, 2012.
- [98] Qiu, D.Y., Da Jornada, F.H. & Louie, S.G., Optical Spectrum of MoS2: Many-Body Effects and Diversity of Exciton States, Physical Review Letters, 111(21), 216805, 2013.
- [99] Wang, G., Marie, X., Gerber, I., Amand, T., Lagarde, D., Bouet, L., Vidal, M., Balocchi, A. & Urbaszek, B., Giant Enhancement of the Optical Second-Harmonic Emission of WSe 2 Monolayers by Laser Excitation at Exciton Resonances, Physical Review Letters, 114(9), 097403, 2015.
- [100] Zhang, C., Johnson, A., Hsu, C.L., Li, L.J. & Shih, C.K., Direct Imaging of Band Profile in Single Layer MoS2 on Graphite: Quasiparticle Energy Gap, Metallic Edge States, and Edge Band Bending, Nano Letters, 14(5), pp. 2443-2447, 2014.
- [101] Ye, Z., Cao, T., O'brien, K., Zhu, H., Yin, X., Wang, Y., Louie, S.G. & Zhang, X., *Probing Excitonic Dark States in Single-layer Tungsten Disulphide,* Nature, **513**(7517), pp. 214-218, 2014.
- [102] He, K., Kumar, N., Zhao, L., Wang, Z., Mak, K.F., Zhao, H. & Shan, J., *Tightly Bound Excitons in Monolayer WSe2*, Physical Review Letters, **113**(2), 026803, 2014.
- [103] Chernikov, A., Berkelbach, T.C., Hill, H.M., Rigosi, A., Li, Y., Aslan, B., Reichman, D.R., Hybertsen, M.S. & Heinz, T.F., *Exciton Binding Energy and Nonhydrogenic Rydberg Series in Monolayer WS2*, Physical Review Letters, **113**(7), 076802, 2014.
- [104] Berkelbach, T.C., Hybertsen, M.S. & Reichman, D.R., *Theory of Neutral and Charged Excitons in Monolayer Transition Metal Dichalcogenides,* Physical Review B, **88**(4), 045318, 2013.
- [105] Ugeda, M.M., Bradley, A.J., Shi, S.F., Da Jornada, F.H., Zhang, Y., Qiu, D.Y., Ruan, W., Mo, S.K., Hussain, Z., Shen, Z.X., Wang, F., Louie, S.G. & Crommie, M.F., Giant Bandgap Renormalization and Excitonic Effects in a Monolayer Transition Metal Dichalcogenide Semiconductor, Nature Materials, 13(12), pp. 1091-1095, 2014.
- [106] Singh, S., Sharma, A.K., Lohia, P. & Dwivedi, D.K., Theoretical Analysis of Sensitivity Enhancement of Surface Plasmon Resonance Biosensor with Zinc Oxide and Blue Phosphorus/Mos2 Heterostructure, Optik, **244**, pp. 167618, 2021.
- [107] Jiao, L., Ma, F., Wang, X., Li, Z., Hu, Z. & Yin, Q., Quinolinediol Molecule Electrode and MXene for Asymmetric Supercapacitors with Efficient Energy Storage, ACS Applied Energy Materials, 4(8), pp. 7811-7820, 2021.
- [108] Anasori, B., Lukatskaya, M.R. & Gogotsi, Y., 2D Metal Carbides and Nitrides (Mxenes) for Energy Storage, Nature Reviews Materials, 2(2), pp. 1-17, 2017.
- [109] Mustakeem, M., El-Demellawi, J.K., Obaid, M., Ming, F., Alshareef, H.N. & Ghaffour, N., *MXene-coated Membranes for Autonomous Solar-Driven Desalination,* ACS Applied Materials & Interfaces, **14**(4), pp. 5265-5274, 2022.

[110] Wang, Y., Nie, J., He, Z., Zhi, Y., Ma, X. & Zhong, P., *Ti3C2T x MXene Nanoflakes Embedded with Copper Indium Selenide Nanoparticles for Desalination and Water Purification through High-Efficiency Solar-Driven Membrane Evaporation*, ACS Applied Materials & Interfaces, **14**(4), pp. 5876-5886, 2022.

- [111] Mehdi Aghaei, S., Aasi, A. & Panchapakesan, B., Experimental and Theoretical Advances in MXene-based Gas Sensors, ACS Omega, 6(4), pp. 2450-2461, 2021.
- [112] Jin, L., Wu, C., Wei, K., He, L., Gao, H., Zhang, H., Zhang, K., Asiri, A.M., Alamry, K.A., Yang, L. & Chu, X., Polymeric Ti3C2T x MXene Composites for Room Temperature Ammonia Sensing, ACS Applied Nano Materials, **3**(12), pp. 12071-12079, 2020.
- [113] Fan, Z., He, H., Yu, J., Liu, L., Liu, Y. & Xie, Z., Lightweight Three-Dimensional Cellular Mxene Film for Superior Energy Storage and Electromagnetic Interference Shielding, ACS Applied Energy Materials, **3**(9), pp. 8171-8178, 2020.
- [114] Liu, C., Wei, X., Hao, S., Zong, B., Chen, X., Li, Z. & Mao, S., Label-Free, Fast Response, and Simply Operated Silver Ion Detection with a Ti3C2Tx MXene Field-Effect Transistor, Analytical Chemistry, 93(22), pp. 8010-8018, 2021.
- [115] Liu, C., Hao, S., Chen, X., Zong, B. & Mao, S., *High Anti-Interference Ti3C2Tx MXene Field-Effect-Transistor-Based Alkali Indicator*, ACS Applied Materials & Interfaces, **12**(29), pp. 32970-32978, 2020.
- [116] Sajid, M., MXenes: Are They Emerging Materials for Analytical Chemistry Applications? A Review, Analytica Chimica Acta, 1143, pp. 267-280, 2021.
- [117] Karlsson, L.H., Birch, J., Halim, J., Barsoum, M.W. & Persson, P.O., *Atomically Resolved Structural and Chemical Investigation of Single Mxene Sheets,* Nano Letters, **15**(8), pp. 4955-4960, 2015.
- [118] Wang, X., Shen, X., Gao, Y., Wang, Z., Yu, R., & Chen, L., Atomic-scale Recognition of Surface Structure and Intercalation Mechanism of Ti3C2X, Journal of the American Chemical Society, 137(7), pp. 2715-2721, 2015.
- [119] Halim, J., Kota, S., Lukatskaya, M.R., Naguib, M., Zhao, M.Q., Moon, E.J., Pitock, J., Nanda, J., May, S.J., Gogotsi, Y. & Barsoum, M.W., Synthesis and Characterization of 2D Molybdenum Carbide (MXene), Advanced Functional Materials, 26(18), pp. 3118-3127, 2016.
- [120] Anasori, B., Xie, Y., Beidaghi, M., Lu, J., Hosler, B. C., Hultman, L., Kent, P.R.C., Gogotsi, Y. & Barsoum, M. W., Two-dimensional, Ordered, Double Transition Metals Carbides (MXenes), ACS Nano, 9(10), pp. 9507-9516, 2015.
- [121] Naguib, M., Kurtoglu, M., Presser, V., Lu, J., Niu, J., Heon, M., Hultman, L., Gogotsi, Y. & Barsoum, M.W., Two-dimensional Nanocrystals Produced by Exfoliation of Ti3AlC2, Advanced Materials, 23(37), pp. 4248-4253, 2011.
- [122] Weng, H., Ranjbar, A., Liang, Y., Song, Z., Khazaei, M., Yunoki, S., Arai, M., Kawazoe, Y., Fang, Z. & Dai, X., Large-gap Two-dimensional Topological Insulator in Oxygen Functionalized MXene, Physical Review B, 92(7), 075436, 2015.
- [123] Si, C., Jin, K. H., Zhou, J., Sun, Z. & Liu, F., Large-gap Quantum Spin Hall state in MXenes: D-band Topological Order in a Triangular Lattice, Nano Letters, 16(10), pp. 6584-6591, 2016.
- [124] Khazaei, M., Ranjbar, A., Arai, M., Sasaki, T. & Yunoki, S., *Electronic Properties and Applications of MXenes: A Theoretical Review,* Journal of Materials Chemistry C, **5**(10), pp. 2488-2503, 2017.
- [125] Gao, L., Li, C., Huang, W., Mei, S., Lin, H., Ou, Q., Zhang, Y., Guo, J., Zhang, F., Xu, S. & Zhang, H., MXene/Polymer Membranes: Synthesis, Properties, and Emerging Applications, Chemistry of Materials, 32(5), pp. 1703-1747, 2020.
- [126] Li, L., Effects of the Interlayer Interaction and Electric Field on the Band Gap of Polar Bilayers: A Case Study of Sc₂CO₂, The Journal of Physical Chemistry C, **120**(43), pp. 24857-24865, 2016.
- [127] Lee, Y., Hwang, Y., Cho, S.B. & Chung, Y.C., Achieving a Direct Band Gap in Oxygen Functionalized-monolayer Scandium Carbide by Applying an Electric Field, Physical Chemistry Chemical Physics, 16(47), pp. 26273-26278, 2014.
- [128] Lee, Y., Cho, S.B. & Chung, Y.C., *Tunable Indirect to Direct Band Gap Transition of Monolayer Sc₂CO₂ By The Strain Effect,* ACS Applied Materials & Interfaces, **6**(16), pp. 14724-14728, 2014.
- [129] Yu, X.F., Cheng, J.B., Liu, Z.B., Li, Q.Z., Li, W.Z., Yang, X. & Xiao, B., *The Band Gap Modulation of Monolayer Ti 2 CO 2 by Strain*, RSC Advances, **5**(39), pp. 30438-30444, 2015.
- [130] Khazaei, M., Arai, M., Sasaki, T., Chung, C.Y., Venkataramanan, N.S., Estili, M., Sakka, Y. & Kawazoe, Y., Novel Electronic and Magnetic Properties of Two-Dimensional Transition Metal Carbides and Nitrides, Advanced Functional Materials, 23(17), pp. 2185-2192, 2013.

- [131] Halim, J., Lukatskaya, M.R., Cook, K.M., Lu, J., Smith, C.R., Näslund, L.Å., May, S.J., Hultman, L., Gogotsi, Y., Eklund, P. & Barsoum, M. W., *Transparent Conductive Two-Dimensional Titanium Carbide Epitaxial Thin Films*, Chemistry of Materials, **26**(7), pp. 2374-2381, 2014.
- [132] Mariano, M., Mashtalir, O., Antonio, F.Q., Ryu, W.H., Deng, B., Xia, F., Gogotsi, Y. & Taylor, A.D., Solution-Processed Titanium Carbide Mxene Films Examined as Highly Transparent Conductors, Nanoscale, 8(36), pp. 16371-16378, 2016.
- [133] Berdiyorov, G.R., Optical Properties of Functionalized Ti3C2T2 (T= F, O, OH) MXene: First-principles Calculations, AIP Advances, 6(5), 2016.
- [134] Xie, Y. & Kent, P.R.C., Hybrid Density Functional Study of Structural and Electronic Properties of Functionalized Ti n+ 1 X n (X= C, N) Monolayers, Physical Review B, 87(23), 235441, 2013.
- [135] Hantanasirisakul, K. & Gogotsi, Y., Electronic and Optical Properties of 2D Transition Metal Carbides and Nitrides (MXenes), Advanced Materials, 30(52), 1804779, 2018.
- [136] Fu, B., Sun, J., Wang, C., Shang, C., Xu, L., Li, J. & Zhang, H., *MXenes: Synthesis, Optical Properties, and Applications in Ultrafast Photonics,* Small, **17**(11), 2006054, 2021.
- [137] Agravat, D., Patel, S.K., Almawgani, A.H., Irfan, M., Armghan, A. & Taya, S.A., *Graphite-based Surface Plasmon Resonance Structure using Al₂O₃-TiO₂-ZrO₂ Materials for Solar Thermal Absorption, Plasmonics, pp. 1-12, 2023.*
- [138] Chung, K., Lee, J.S., Kim, E., Lee, K.E., Kim, K., Lee, J., Kim, D., Kim, S.O., Jeon, S., Park, H., Kim, D.W. & Kim, D.H., Enhancing the Performance of Surface Plasmon Resonance Biosensor via Modulation of Electron Density at the Graphene–Gold Interface, Advanced Materials Interfaces, 5(19), 1800433, 2018.
- [139] Saleviter, S., Fen, Y.W., Daniyal, W.M.E.M.M., Abdullah, J., Sadrolhosseini, A.R. & Omar, N.A.S., *Design and Analysis of Surface Plasmon Resonance Optical Sensor for Determining Cobalt Ion Based on Chitosan-Graphene Oxide Decorated Quantum Dots-Modified Gold Active Layer, Optics Express*, **27**(22), pp. 32294-32307, 2019.
- [140] Rahman, M.S., Hasan, M.R., Rikta, K.A. & Anower, M.S., A Novel Graphene Coated Surface Plasmon Resonance Biosensor with Tungsten Disulfide (WS2) for Sensing DNA Hybridization, Optical Materials, **75**, pp. 567-573, 2018.
- [141] Rahman, M.S., Anower, M.S., Hasan, M.R., Hossain, M.B. & Haque, M.I., *Design and Numerical Analysis of Highly Sensitive Au-MoS2-Graphene Based Hybrid Surface Plasmon Resonance Biosensor*, Optics Communications, **396**, pp. 36-43, 2017.
- [142] Taya, S.A., Doghmosh, N., Almawgani, A.H., Hindi, A.T., Colak, I., Alqanoo, A.A., Patel, S.K. & Pal, A., Surface Plasmon Resonance Biosensor Based on STO and Graphene Sheets for Detecting Two Commonly Used Buffers: TRIS—Borate-EDTA and Dulbecco Phosphate Buffered Saline, Plasmonics, pp. 1-9, 2023.
- [143] Taya, S.A., Al-Ashi, N.E., Ramahi, O.M., Colak, I. & Amiri, I.S., Surface Plasmon Resonance-Based Optical Sensor Using a Thin Layer of Plasma, JOSA B, 38(8), pp. 2362-2367, 2021.
- [144] Meshginqalam, B., Ahmadi, M.T., Ismail, R. & Sabatyan, A., *Graphene/graphene Oxide-Based Ultrasensitive Surface Plasmon Resonance Biosensor*, Plasmonics, **12**, pp. 1991-1997, 2017.
- [145] Verma, A., Prakash, A. & Tripathi, R., *Performance Analysis of Graphene Based Surface Plasmon Resonance Biosensors for Detection of Pseudomonas-Like Bacteria*, Optical and Quantum Electronics, **47**, pp. 1197-1205, 2015.
- [146] Bhavsar, K., Prabhu, R. & Pollard, P., *Ultrasensitive Graphene Coated SPR Sensor for Biosensing Applications*, Optical Sensors, **9506**, pp. 173-178, SPIE, 2015.
- [147] Panda, A., Pukhrambam, P.D. & Keiser, G., Performance Analysis of Graphene-Based Surface Plasmon Resonance Biosensor for Blood Glucose and Gas Detection, Applied Physics A, 126(3), 2020. doi: 10.1007/s00339-020-3328-8.
- [148] Pal, S., Verma, A., Prajapati, Y.K. & Saini, J.P., *Influence of Black Phosphorous on Performance of Surface Plasmon Resonance Biosensor*, Optical and Quantum Electronics, **49**, pp. s1-13, 2017.
- [149] Wang, L., Zhu, C., Han, L., Jin, L., Zhou, M. & Dong, S., Label-free, Regenerative and Sensitive Surface Plasmon Resonance and Electrochemical Aptasensors Based on Graphene, Chemical Communications, 47(27), pp. 7794-7796, 2011.
- [150] Cai, L., Zhan, R., Pu, K.Y., Qi, X., Zhang, H., Huang, W. & Liu, B., Butterfly-shaped Conjugated Oligoelectrolyte/Graphene Oxide Integrated Assay for Light-Up Visual Detection of Heparin, Analytical Chemistry, 83(20), pp. 7849-7855, 2011.
- [151] Gilje, S., Han, S., Wang, M., Wang, K.L. & Kaner, R.B., A Chemical Route to Graphene for Device Applications, Nano Letters, **7**(11), pp. 3394-3398, 2007.

[152] Wu, Q., Sun, Y., Ma, P., Zhang, D., Li, S., Wang, X. & Song, D., Gold Nanostar-Enhanced Surface Plasmon Resonance Biosensor Based on Carboxyl-Functionalized Graphene Oxide, Analytica Chimica Acta, 913, pp. 137-144, 2016.

- [153] Subramanian, P., Barka-Bouaifel, F., Bouckaert, J., Yamakawa, N., Boukherroub, R. & Szunerits, S., Graphene-coated Surface Plasmon Resonance Interfaces for Studying the Interactions between Bacteria and Surfaces, ACS Applied Materials & Interfaces, 6(8), pp. 5422-5431, 2014.
- [154] Parab, H.J., Jung, C., Lee, J.H. & Park, H.G., A Gold Nanorod-Based Optical DNA Biosensor for the Diagnosis of Pathogens, Biosensors and Bioelectronics, 26(2), pp. 667-673, 2010.
- [155] Zhang, J., Sun, Y., Xu, B., Zhang, H., Gao, Y., Zhang, H. & Song, D., A Novel Surface Plasmon Resonance Biosensor Based on Graphene Oxide Decorated with Gold Nanorod–Antibody Conjugates for Determination of Transferrin, Biosensors and Bioelectronics, 45, pp. 230-236, 2013.
- [156] Loh, K.P., Bao, Q., Eda, G. & Chhowalla, M., *Graphene Oxide as a Chemically Tunable Platform for Optical Applications*, Nature Chemistry, **2**(12), pp. 1015-1024, 2010.
- [157] Jana, D., Matti, C., He, J. & Sagle, L., Capping Agent-Free Gold Nanostars Show Greatly Increased Versatility and Sensitivity for Biosensing, Analytical Chemistry, 87(7), pp. 3964-3972, 2015.
- [158] Rahman, M.S. & Abdulrazak, L.F., *Utilization of a Phosphorene-Graphene/TMDC Heterostructure in a Surface Plasmon Resonance-Based Fiber Optic Biosensor*, Photonics and Nanostructures-Fundamentals and Applications, **35**, 100711, 2019.
- [159] Pal, S., Verma, A., Raikwar, S., Prajapati, Y.K. & Saini, J.P., Detection of DNA Hybridization Using Graphene-Coated Black Phosphorus Surface Plasmon Resonance Sensor, Applied Physics A, **124**, pp. 1-11, 2018.
- [160] Hu, W., He, G., Zhang, H., Wu, X., Li, J., Zhao, Z., Qiao, Y., Lu, Z., Liu, Y. & Li, C. M., Polydopamine-functionalization of Graphene Oxide to Enable Dual Signal Amplification for Sensitive Surface Plasmon Resonance Imaging Detection of Biomarker, Analytical Chemistry, 86(9), pp. 4488-4493, 2014.
- [161] Sadrolhosseini, A. R., Shafie, S., Rashid, S. A., & Mahdi, M. A., Surface Plasmon Resonance Measurement of Arsenic in Low Concentration Using Polypyrrole-Graphene Quantum Dots Layer, Measurement, 173, 108546, 2021.
- [162] Singh, M., Holzinger, M., Tabrizian, M., Winters, S., Berner, N.C., Cosnier, S. & Duesberg, G.S., Noncovalently Functionalized Monolayer Graphene for Sensitivity Enhancement of Surface Plasmon Resonance Immunosensors, Journal of the American Chemical Society, 137(8), pp. 2800-2803, 2015.
- [163] Primo, E.N., Kogan, M.J., Verdejo, H.E., Bollo, S., Rubianes, M.D. & Rivas, G.A., Label-free Graphene Oxide-Based Surface Plasmon Resonance Immunosensor for the Quantification of Galectin-3, A Novel Cardiac Biomarker, ACS Applied Materials & Interfaces, 10(28), pp. 23501-23508, 2018.
- [164] Lee, H., Dellatore, S.M., Miller, W.M. & Messersmith, P.B., *Mussel-inspired Surface Chemistry for Multifunctional Coatings*, Science, **318**(5849), pp. 426-430, 2007.
- [165] Tan, F., Cong, L., Li, X., Zhao, Q., Zhao, H., Quan, X. & Chen, J., *An Electrochemical Sensor Based on Molecularly Imprinted Polypyrrole/Graphene Quantum Dots Composite for Detection of Bisphenol a in Water Samples,* Sensors and Actuators B: Chemical, **233**, pp. 599-606, 2016.
- [166] Zhou, X., Ma, P., Wang, A., Yu, C., Qian, T., Wu, S. & Shen, J., *Dopamine Fluorescent Sensors Based on Polypyrrole/Graphene Quantum Dots Core/Shell Hybrids,* Biosensors and Bioelectronics, **64**, pp. 404-410, 2015.
- [167] Sadrolhosseini, A.R., Rashid, S.A., Jamaludin, N., Noor, A.S.M. & Isloor, A.M., *Surface Plasmon Resonance Sensor Using Polypyrrole-Chitosan/Graphene Quantum Dots Layer for Detection of Sugar*, Materials Research Express, **6**(7), 075028, 2019.
- [168] Almawgani, A.H., Taya, S.A., Abutailkh, M.A., Abohassan, K.M., Hindi, A.T., Colak, I., Pal, A. & Patel, S. K., Development of a Biosensor Based on a Surface Plasmon Resonance Structure Comprising Strontium Titanate, Graphene and Affinity Layers for Malaria Diagnosis, Modern Physics Letters B, 2350190, 2023.
- [169] Anas, N.A.A., Fen, Y.W., Yusof, N.A., Omar, N.A.S., Daniyal, W.M.E.M.M. & Ramdzan, N.S.M., *Highly Sensitive Surface Plasmon Resonance Optical Detection of Ferric Ion Using CTAB/Hydroxylated Graphene Quantum Dots Thin Film,* Journal of Applied Physics, **128**(8), 2020.
- [170] Zhang, H., Chhowalla, M. & Liu, Z., 2D Nanomaterials: Graphene and Transition Metal Dichalcogenides, Chemical Society Reviews, 47(9), pp. 3015-3017, 2018.
- [171] Wang, M., Huo, Y., Jiang, S., Zhang, C., Yang, C., Ning, T., Liu, X., Liu, C., Zhang, W. & Man, B., Theoretical Design of a Surface Plasmon Resonance Sensor with High Sensitivity and High Resolution Based on Graphene–WS 2 Hybrid Nanostructures and Au–Ag Bimetallic Film, RSC Advances, 7(75), pp. 47177-47182, 2017.

- [172] Zadeh, S.Z., Keshavarz, A. & Zamani, N., Performance Enhancement of Surface Plasmon Resonance Biosensors Based on Noble Metals-Graphene-WS2 at Visible and Near-Infrared Wavelengths, Plasmonics, 15(2), pp. 309-317, 2020.
- [173] Rouf, H.K. & Haque, T., Sensitivity Enhancement of Graphene-MoSe2–Based SPR Sensor Using Ti Adhesion Layer for Detecting Biological Analytes, Plasmonics, **16**(6), pp. 1945-1954, 2021.
- [174] Homola, J., Surface Plasmon Resonance Sensors for Detection of Chemical And Biological Species, Chemical Reviews, **108**(2), pp. 462-493, 2008.
- [175] Verma, R., Gupta, B.D. & Jha, R., Sensitivity Enhancement of a Surface Plasmon Resonance Based Biomolecules Sensor Using Graphene and Silicon Layers, Sensors and Actuators B: Chemical, 160(1), pp. 623-631, 2011.
- [176] Ouyang, Q., Zeng, S., Jiang, L., Hong, L., Xu, G., Dinh, X.Q., Qian, J., He, S., Qu, J., Coquet, P. & Yong, K.T., Sensitivity Enhancement of Transition Metal Dichalcogenides/Silicon Nanostructure-Based Surface Plasmon Resonance Biosensor, Scientific Reports, 6(1), 28190, 2016.
- [177] Xu, Y., Ang, Y.S., Wu, L. & Ang, L.K., High Sensitivity Surface Plasmon Resonance Sensor Based on Two-Dimensional MXene and Transition Metal Dichalcogenide: A Theoretical Study, Nanomaterials, 9(2), 165, 2019.
- [178] Şar, H., Özden, A., Demiroğlu, İ., Sevik, C., Perkgoz, N.K. & Ay, F., Long-Term Stability Control of CVD-Grown Monolayer MoS2, Physica Status Solidi (RRL)—Rapid Research Letters, 13(7), 1800687, 2019.
- [179] Wu, D., Shi, J., Zheng, X., Liu, J., Dou, W., Gao, Y., Yuan, X., Ouyang, F. & Huang, H., *CVD Grown MoS2 Nanoribbons on MoS2 Covered Sapphire (0001) without Catalysts,* Physica Status Solidi (RRL)–Rapid Research Letters, **13**(7), 1900063, 2019.
- [180] Xiang, M., Liu, H., Huang, C., Li, Y., Zeng, H. & Shao, X., Mo Doping Assisting the CVD Synthesis of Size-Controlled, Uniformly Distributed Single-Layer Mos2 on Rutile TiO2 (110), ACS Applied Materials & Interfaces, 12(30), pp. 34378-34387, 2020.
- [181] Liu, H., Chen, L., Zhu, H., Sun, Q. Q., Ding, S. J., Zhou, P. & Zhang, D. W., Atomic Layer Deposited 2D MoS 2 Atomic Crystals: From Material to Circuit, Nano Research, 13, pp. 1644-1650, 2020.
- [182] Shen, C., Raza, M. H., Amsalem, P., Schultz, T., Koch, N. & Pinna, N., *Morphology-controlled MoS 2 by Low-Temperature Atomic Layer Deposition*, Nanoscale, **12**(39), pp. 20404-20412, 2020.
- [183] Yang, J. & Liu, L., Nanotribological Properties of 2-D MoS2 on Different Substrates Made By Atomic Layer Deposition (ALD), Applied Surface Science, **502**, 144402, 2020.
- [184] Ghidiu, M., Halim, J., Kota, S., Bish, D., Gogotsi, Y. & Barsoum, M. W., *Ion-exchange and Cation Solvation Reactions in Ti3C2 MXene*, Chemistry of Materials, **28**(10), pp. 3507-3514, 2016.
- [185] Golub, A.S., Zubavichus, Y.V., Slovokhotov, Y.L. & Novikov, Y.N., *Monolayer Dispersions of Transition-Metal Dichalcogenides in the Synthesis of Intercalation Compounds, Usp. Khim*, **172**(2), pp. 138-158, 2003.
- [186] Benavente, E., Santa Ana, M.A., Mendizábal, F. & González, G., *Intercalation Chemistry of Molybdenum Disulfide*, Coordination Chemistry Reviews, **224**(1-2), pp. 87-109, 2002.
- [187] Liu, K., Zhang, J., Jiang, J., Xu, T., Wang, S., Chang, P., Zhang, Z., Ma, J. & Liu, T., Multi-layer Optical Fiber Surface Plasmon Resonance Biosensor Based on a Sandwich Structure of Polydopamine-MoSe 2@ Au nanoparticles-polydopamine, Biomedical Optics Express, 11(12), pp. 6840-6851, 2020.
- [188] Jia, Q., Huang, X., Wang, G., Diao, J. & Jiang, P., MoS2 Nanosheet Superstructures Based Polymer Composites for High-Dielectric and Electrical Energy Storage Applications, The Journal of Physical Chemistry C, 120(19), pp. 10206-10214, 2016.
- [189] Kim, N.H., Choi, M., Kim, T.W., Choi, W., Park, S.Y. & Byun, K. M., Sensitivity and Stability Enhancement of Surface Plasmon Resonance Biosensors Based on a Large-Area Ag/MoS2 Substrate, Sensors, 19(8), 1894, 2019.
- [190] Youngá Chung, D., ChuláHam, H. & JongáYoo, S., Edge-exposed MoS2 Nano-Assembled Structures as Efficient Electrocatalysts for Hydrogen Evolution Reaction, Nanoscale, 6(4), pp. 2131-2136, 2014.
- [191] Zhang, D., Jiang, C., Li, P. & Sun, Y. E., Layer-by-layer Self-assembly of Co3O4 Nanorod-Decorated MoS2 Nanosheet-Based Nanocomposite toward High-Performance Ammonia Detection, ACS Applied Materials & Interfaces, 9(7), pp. 6462-6471, 2017.
- [192] Filbrun, S.L., Filbrun, A.B., Lovato, F.L., Oh, S.H., Driskell, E.A. & Driskell, J.D., Chemical Modification of Antibodies Enables the Formation of Stable Antibody–Gold Nanoparticle Conjugates for Biosensing, Analyst, 142(23), pp. 4456-4467, 2017.

[193] Kaushik, S., Tiwari, U.K., Pal, S.S., & Sinha, R.K., Rapid Detection of Escherichia Coli Using Fiber Optic Surface Plasmon Resonance Immunosensor Based on Biofunctionalized Molybdenum Disulfide (MoS2) Nanosheets, Biosensors and Bioelectronics, 126, pp. 501-509, 2019.

- [194] Lopez-Sanchez, O., Lembke, D., Kayci, M., Radenovic, A. & Kis, A., *Ultrasensitive Photodetectors based on Monolayer MoS2, Nature Nanotechnology*, **8**(7), pp. 497-501, 2013.
- [195] Zhang, Y., Wang, L., Zhang, N. & Zhou, Z., Adsorptive Environmental Applications of MXene Nanomaterials: A Review, RSC Advances, 8(36), pp. 19895-19905, 2018.
- [196] Sang, X., Xie, Y., Lin, M.W., Alhabeb, M., Van Aken, K.L., Gogotsi, Y., Kent, P.R.C., Xiao, K. & Unocic, R.R., Atomic Defects in Monolayer Titanium Carbide (Ti3C2T x) MXene, ACS Nano, 10(10), pp. 9193-9200, 2016.
- [197] Lipatov, A., Alhabeb, M., Lukatskaya, M.R., Boson, A., Gogotsi, Y. & Sinitskii, A., Effect of Synthesis on Quality, Electronic Properties and Environmental Stability of Individual Monolayer Ti3C2 MXene Flakes, Advanced Electronic Materials, 2(12), 1600255, 2016.
- [198] Khazaei, M., Ranjbar, A., Ghorbani-Asl, M., Arai, M., Sasaki, T., Liang, Y. & Yunoki, S., *Nearly Free Electron States in MXenes*, Physical Review B, **93**(20), 205125, 2016.
- [199] Peng, Q., Guo, J., Zhang, Q., Xiang, J., Liu, B., Zhou, A., Liu, R. & Tian, Y., *Unique Lead Adsorption Behavior of Activated Hydroxyl Group in Two-Dimensional Titanium Carbide,* Journal of the American Chemical Society, **136**(11), pp. 4113-4116, 2014.
- [200] Urbankowski, P., Anasori, B., Makaryan, T., Er, D., Kota, S., Walsh, P.L., Zhao, M., Shenoy, V.B., Barsoum, M.W. & Gogotsi, Y., *Synthesis of Two-dimensional Titanium Nitride Ti 4 N 3 (MXene)*, Nanoscale, **8**(22), pp. 11385-11391, 2016.
- [201] Anasori, B., Lukatskaya, M.R. & Gogotsi, Y., 2D Metal Carbides and Nitrides (MXenes) for Energy Storage, Nature Reviews Materials, 2(2), pp. 1-17, 2017.
- [202] Wu, L., You, Q., Shan, Y., Gan, S., Zhao, Y., Dai, X. & Xiang, Y., Few-layer Ti3C2Tx MXene: A Promising Surface Plasmon Resonance Biosensing Material to Enhance the Sensitivity, Sensors and Actuators B: Chemical, 277, pp. 210-215, 2018.
- [203] Gan, S., Ruan, B., Xiang, Y. & Dai, X., Highly Sensitive Surface Plasmon Resonance Sensor Modified with 2D Ti₂C MXene for Solution Detection, IEEE Sensors Journal, 21(1), pp. 347-352, 2020.
- [204] Luo, S., Patole, S., Anwer, S., Li, B., Delclos, T., Gogotsi, O., Zahorodna V., Balitskyi V. & Liao, K., *Tensile Behaviors of Ti3C2Tx (MXene) Films, Nanotechnology*, **31**(39), 395704, 2020.
- [205] Srivastava, A., Verma, A., Das, R. & Prajapati, Y.K., A Theoretical Approach to Improve the Performance of SPR Biosensor Using Mxene and Black Phosphorus, Optik, **203**, 163430, 2020.
- [206] Kumar, R., Pal, S., Pal, N., Mishra, V. & Prajapati, Y.K., High-Performance Bimetallic Surface Plasmon Resonance Biochemical Sensor Using a Black Phosphorus–Mxene Hybrid Structure, Applied Physics A, 127(4), 259, 2021.
- [207] Srivastava, A., & Prajapati, Y. K., Surface Plasmon Resonance (SPR)-Based Biosensor Using Mxene as a BRE Layer and Magnesium Oxide (Mgo) as an Adhesion Layer, Journal of Materials Science: Materials in Electronics, pp. 1-10, 2021.
- [208] Kumar, R., Pal, S., Prajapati, Y.K., & Saini, J.P., Sensitivity Enhancement of Mxene Based SPR Sensor Using Silicon: Theoretical Analysis, Silicon, 13, pp. 1887-1894, 2021.
- [209] Liu, H., Neal, A. T., Zhu, Z., Luo, Z., Xu, X., Tománek, D. & Ye, P.D., *Phosphorene: An Unexplored 2D Semiconductor with a High Hole Mobility, ACS Nano,* **8**(4), pp. 4033-4041, 2014.
- [210] Cho, S.Y., Lee, Y., Koh, H.J., Jung, H., Kim, J.S., Yoo, H.W., Kim, J. & Jung, H.T., Superior Chemical Sensing Performance of Black Phosphorus: Comparison with MoS2 and Graphene, Advanced Materials, 28(32), pp. 7020-7028, 2016.
- [211] Wu, L., Guo, J., Wang, Q., Lu, S., Dai, X., Xiang, Y. & Fan, D., Sensitivity Enhancement by Using Few-Layer Black Phosphorus-Graphene/TMDCs Heterostructure in Surface Plasmon Resonance Biochemical Sensor, Sensors and Actuators B: Chemical, 249, pp. 542-548, 2017.
- [212] Pal, S., Verma, A., Saini, J. P., & Prajapati, Y. K., Sensitivity Enhancement Using Silicon-Black Phosphorus-TDMC Coated Surface Plasmon Resonance Biosensor, let Optoelectronics, 13(4), pp. 196-201, 2019.
- [213] Hakami, J., Abassi, A. & Dhibi, A., *Performance Enhancement of Surface Plasmon Resonance Sensor Based on Ag-Tio2-Mapbx3-Graphene for the Detection of Glucose in Water*, Optical and Quantum Electronics, **53**(4), 164, 2021.
- [214] Polavarapu, L., Nickel, B., Feldmann, J. & Urban, A.S., Advances in Quantum-Confined Perovskite Nanocrystals for Optoelectronics, Advanced Energy Materials, 7(16), 1700267, 2017.

- [215] Jagielski, J., Kumar, S., Yu, W. Y., & Shih, C. J., Layer-Controlled Two-Dimensional Perovskites: Synthesis and Optoelectronics, Journal of Materials Chemistry C, 5(23), pp. 5610-5627, 2017.
- [216] Hong, K., Van Le, Q., Kim, S.Y., & Jang, H.W., Low-Dimensional Halide Perovskites: Review and Issues, Journal of Materials Chemistry C, **6**(9), pp. 2189-2209, 2018.
- [217] Chen, S., & Shi, G., *Two-Dimensional Materials for Halide Perovskite-Based Optoelectronic Devices*, Advanced Materials, **29**(24), 1605448, 2017.
- [218] Zhao, Y., Gan, S., Wu, L., Zhu, J., Xiang, Y. & Dai, X., GeSe nanosheets modified surface plasmon resonance sensors for enhancing sensitivity, Nanophotonics, **9**(2), pp. 327-336, 2020.
- [219] Miah, M.A.R. & Shaikh, A.A., WS 2-CH 3 NH 3 Pbl 3 Perovskite Nanostructure based Bimetallic Surface Plasmon Resonance Biosensor with High Sensitivity and High Resolution, in 2019 Joint 8th International Conference on Informatics, Electronics & Vision (ICIEV) and 2019 3rd International Conference on Imaging, Vision & Pattern Recognition (icIVPR), pp. 234-237, 2019.
- [220] Srivastava, A., Das, R. & Prajapati, Y.K., Effect Of Perovskite Material on Performance of Surface Plasmon Resonance Biosensor, IET Optoelectronics, **14**(5), pp. 256-265, 2020.
- [221] Khan, A.F., Brownson, D.A., Randviir, E.P., Smith, G.C. & Banks, C.E., 2D Hexagonal Boron Nitride (2D-Hbn) Explored for the Electrochemical Sensing of Dopamine, Analytical Chemistry, 88(19), pp. 9729-9737, 2016.
- [222] Yola, M.L. & Atar, N., Gold Nanoparticles/Two-Dimensional (2D) Hexagonal Boron Nitride Nanosheets Including Diethylstilbestrol Imprinted Polymer: Electrochemical Detection in Urine Samples and Validation, Journal of The Electrochemical Society, **165**(14), H897, 2018.
- [223] Özkan, A., Atar, N. & Yola, M.L., Enhanced Surface Plasmon Resonance (SPR) Signals Based on Immobilization of Core-Shell Nanoparticles Incorporated Boron Nitride Nanosheets: Development of Molecularly Imprinted SPR Nanosensor for Anticancer Drug, Etoposide, Biosensors and Bioelectronics, 130, pp. 293-298, 2019.

Manuscript Received: 2 July 2023 Revised Manuscript Received: 3 October 2023 Accepted Manuscript: 18 October 2023